Faculty of Engineering of the University of Porto

Towards novel human sweat sensors

Bruno Santos

Dissertation carried for degree of Master in biomedical engineering

Supervisor: Professor Doutor João Paulo Cunha,
Faculty of Engineering of the University of Porto

June 2019

Abstract

Sweat is a complex concoction of organic and inorganic components in an aqueous solution that is unique to mammals including humans. Despite its secretion being attributed to thermo-regulatory processes, nowadays, there is a deeper interest in sweat as a potential biological marker. This is due to the fact that sweat's components encompass a wide range of medically relevant biomarkers such as NaCl, urea and lactic acid. Recent studies have shown that some of the biomarkers found in sweat have intricate correlations to specific physical conditions and pathologies. This way, newly non-invasive methods for monitorization and diagnosis of certain conditions using key biomarkers sampled from sweat are on the rise. Despite showing promising results, these rely heavily on colorimetrical and electrochemical approaches, which have several limitations.

This dissertation work aims at determining the potential of several distinct optical techniques for human sweat monitoring with the perspective of incorporation in wearable devices. In this sense, a selection of low-cost optical sensors and optical fiber were assessed using relevant sweat biomarkers and a custom formulation of artificial sweat. Furthermore, wide-range spectral techniques (UV-VIS and ATR-FTIR) were also employed to characterize the artificial sweat solutions and its individual components. Moreover, literature review was also heavily conducted on the subject to acquire insight on the nature of sweat's composition and to document state-of-the-art works that pushed the concept of sweat monitorization forward.

Results of the sensor assessment suggested the AS7262, AS7263 and MAX30101 to be the most suitable sensors for sweat monitoring as they consistently displayed coherent and statistically significant behavior between the tested solutions ($p<0.001$). They were successfully able to discern the single compound solutions from water, to discern artificial sweat solution from water and able to discriminate different artificial sweat concentrations in the biological range. Conversely, the optic fiber setup used did not possess the required resolution to convey statistically significant measurements.

Although the UV-VIS results could not produce a spectrum for any of the tested compounds, the ATR-FTIR technique produced very interesting results as both organic biomarkers were profiled in the IR region which revealed interest transmittance peaks for both urea and lactic acid at 1468cm^{-1} and 1132cm^{-1} respectively. Furthermore, the artificial sweat spectrum analysis suggested the existence of an active effect of NaCl in the amplitude of a specific peak (595cm^{-1}). These results foreshadow the exploration of sweat sensors in the IR range.

Future studies should aim at improving the current optical techniques by improving the overall system sensibility and by exploiting the documented peaks in the IR spectrum.

Resumo

O suor é uma mistura complexa de componentes orgânicos e inorgânicos presente numa solução aquosa que é exclusiva dos mamíferos incluindo humanos. Apesar dos mecanismos subjacentes à sua secreção estarem intimamente associados a fenómenos termo regulatórios, atualmente existe um interesse mais profundo pelo suor como um potencial marcador fisiológico. Isto deve-se ao facto de os componentes presentes no suor englobarem uma vasta gama de biomarcadores clinicamente relevantes como é o caso do NaCl, da ureia e do ácido láctico. Estudos recentes mostraram que alguns dos biomarcadores encontrados no suor apresentam correlações específicas com determinadas patologias e condições físicas. Assim, novos métodos não invasivos para monitorizar o suor estão a surgir, métodos que utilizam biomarcadores específicos para deteção de certas doenças ou estados fisiológicos. Contudo, estes trabalhos sustentam-se unicamente em métodos colorimétricos e electroquímicos que, apesar de promissores, possuem algumas limitações.

Esta dissertação tem como objetivo determinar o potencial de várias técnicas óticas distintas para monitorizar suor humano com vista a uma possível incorporação em dispositivos "wearable". Neste sentido, uma seleção de sensores óticos de baixo custo e de fibra ótica foram avaliados utilizando biomarcadores presentes no suor e uma formulação personalizada de suor sintético. Além disto, duas técnicas de espectrometria de vasta-gama (UV-VIS e ATR-FTIR) foram utilizadas para realizar a caracterização das soluções de suor sintético e dos seus componentes individuais. Adicionalmente, foi realizada uma extensa revisão bibliográfica sobre a matéria de modo a obter conhecimentos sobre a composição natural do suor. Além disso, foi ainda feita a uma revisão do estado-da-arte, nomeadamente analisado os trabalhos que impulsionaram o conceito da monitorização do suor.

Os resultados da avaliação dos sensores sugerem que o AS7262, o AS7263 e o MAX30101 são os sensores mais adequados para monitorizar suor visto que todos apresentaram comportamentos consistentemente coerentes e com significância estatística entre as soluções testadas ($p<0.001$). Estes sensores conseguiram, com sucesso, distinguir as soluções com biomarcadores da água, as soluções do suor sintético da água e ainda conseguiram discriminar diferentes concentrações de suor sintético que se encontravam dentro dos valores encontrados em ambiente biológico. Não obstante, o sistema de fibra ótica não possuía a sensibilidade necessária para realizar medições que fossem dotadas de relevância estatística.

Apesar dos resultados do UV-VIS não evidenciarem nenhum espectro para os componentes testados, os resultados do ATR-FTIR foram muito interessantes visto que ambos biomarcadores orgânicos foram caracterizados na região do infravermelho que revelou picos de transmitância de interesse para a ureia (a 1468cm^{-1}) e para o ácido láctico (a 1132cm^{-1}). Além disto, as análises de

espectro das soluções de suor sintético evidenciaram a existência de um efeito ativo por parte do Cloreto de Sódio na amplitude de um pico específico (595cm^{-1}). Estes resultados pressagiam a exploração de sensores para monitorização de suor na gama dos infravermelhos.

Estudos futuros devem procurar melhorar as técnicas óticas presentes neste estudo melhorando a sensibilidade geral dos sistemas e através da exploração dos picos documentados neste documento na gama dos infravermelhos.

Acknowledgments

Primeiramente, ao meu orientador, professor Dr. João Paulo Cunha pelo apoio no desenvolvimento desta dissertação e por me acolher no BRAIN group onde tive a oportunidade de conhecer pessoas novas e integrar novos conhecimentos.

Ao professor Joaquim L Faria cuja ajuda foi fulcral para o desenvolvimento da parte prática da minha dissertação e que interveio ativamente no seu rumo apesar de não ter de o fazer, considero-o por isso, um verdadeiro orientador.

Ao Guilherme Braga, que me ajudou bastante a familiarizar-me com o desafio em questão e ao Daniel Malafaia, que não só me ajudou na integração da equipa, mas que também se mostrou sempre disponível para atender às minhas dúvidas e dificuldades.

Aos meus pais, que as são as pessoas mais importantes da minha vida, um muito obrigado. Sem vocês nunca teria chegado onde cheguei nem conquistar o que conquistei. Vocês são a razão do meu sucesso e eu espero um dia poder retribuir tudo o que me proporcionam. Esta dissertação é vossa também.

Aos meus caríssimos conterrâneos, o grupo da minha terra, as pessoas com quem cresci! O vosso companheirismo e conselhos (impetuosos, mas honestos) foram fulcrais à retenção da minha sanidade mental, nunca me deixando contemplar o abismo sozinho: Dianel, Mériuh, Simãos, Rosta, Dias, Shuao, Ucra, Rita, um muito MUITO obrigado (sois lindos, cheirais bem e tomais banho).

Ao Congresso MEBiano o grupo que me acolheu de braços abertos no meu regresso à FEUP e que me fizeram acreditar num ambiente académico impulsionado pela união, solidariedade e espírito de sacrifício, sem nunca deixar ninguém para trás: Bia, Cat, Ciclas, Ju, Luís, Marisa, Miguel, Raquel e Tomé, um muito obrigado.

Ao Tiago por me ter ajudado imensamente, mesmo quando não pude estar presente. Um agradecimento especial ao Luís, um grande amigo, mas também um grande mentor, cuja inteligência pode apenas ser equiparada à sua bondade, um sincero obrigado. E finalmente, à Ju, obrigado por todas as pequenas coisas que não vêm escritas em dissertações de mestrado. Somos, de facto, a melhor equipa!!!

"We are thinking on the basest of planes. What we need, are more eyes."

Provost Willem, Bloodborne

Contents

List of Figures

List of tables

Abbreviations, Acronyms and Symbols

List of abbreviations and acronyms

µA	Micro-Ampere
ADC	Analog to Digital Converter
ATR	Attenuated total reflectance
Cm	Centimeter
CMOS	Complementary metal–oxide–semiconductor
FTIR	Fourier-transform infrared spectroscopy
FWHM	Full Width at Half Maximum
GUI	Graphical User Interface
IC	Integrated Circuit
IR	Infrared
LA	Lactic Acid
LED	Light-emitting diode
LGA	Land Grid Array
M	Molar
Mhz	Megahertz
mM	Mili-molar
NIR	Near-Infrared
Nm	Nanometer
PLA	Poly-lactic acid
ROI	Region-of-Interest
SD	Standard deviation
SNR	Signal-to-Noise Ratio
SPAD	Single Photon Avalanche Diode
TIR	Total Internal Reflection
USB	Universal Serial Bus
UV-VIS	Ultraviolet-visible spectroscopy

List of Symbols

ºC	Degree Celsius

Chapter 1

Introduction

In this introductory chapter, a brief overview of the selected topic will be presented as well as the milestones set within this study and their respective intended methodological approaches. Finally, a structural exposition of the matters covered in this study will be given to serve as a more detailed index.

1.1 – Background

Physiology has had an impressive developmental track record over the last few decades. Since the dawn of modern medicine, the understanding of physiology and its mechanisms in humans have been thoroughly scrutinized and exploited to aid medicine in several different ways. The most prominent aspects of this science concern diagnosis and pathological response [1]. Today's commonly known "physiological indicators" greatly contribute to patient diagnosis and monitoring in the XXI century. An assortment of techniques and devices have been developed to identify and measure these indicators.

Many of these techniques and apparatus are well documented and provide accurate measurements on these biological parameters as well as pathological occurrences linked with such indicators (thermometers, sphygmomanometers, electrocardiography, etc.). Despite this, some of these markers are still being overlooked today which may result in the loss of its potential. Sweat is a prime example of the aforementioned case. Several studies have shown that pathologies, physical stress and regional location can drastically alter sweat production, composition and component concentrations [2], [3]. Although these interactions are well documented, sweat is still a very complex concoction that is both hard to replicate in vitro and hard to analyze in vivo.

1.2 – Motivation and technical approach

The trend towards electronic miniaturization and improved photolithography processes had enabled the production of highly integrated circuits (ICs) for portable and easy to manufacture consumer equipment. These new ICs are promising contenders for portable equipment for patient diagnosis.

Optical sensors are a well-known type of devices that explore the physics of electromagnetic radiation to draw tangible relations and convey measurements. These sensors can detect changes in some organic solutions by light refraction, absorption and reflection while simultaneously being simple and non-invasive [4]. Recent studies have shown a clear application of these sensors in a colorimetric approach to sweat characterization using them in combination with pH sensors to estimate ion concentration in sweat [5]. However, in these studies, the role of the optical sensor is purely accessory serving as a complement to the already implemented chemical system. A purely optical system for sweat analysis is yet to be documented.

Furthermore, optical sensors have already been established in the medical community as a viable, cheap and reliable option for certain measurements, such is the case of the well-known oximeter, which uses the same physical principles as the devices used in this study [6].

These newly emerging sensors and technologies can contribute to explore promising ways to evaluate and analyze sweat namely in future wearable devices. This dissertation work will focus on assessing the viability of several optical techniques for sweat monitoring. Relevant sweat compound solutions based on literature and artificial sweat formulations synthesized from these compounds, also found in literature, will be used. Furthermore, two wide-range spectroscopy techniques will be employed to characterize the single compound and artificial sweat solutions.

1.3 – Objectives and planned methodology

Given the sweat's potential as a physiological indicator, the aim of this dissertation is to conduct a proof of concept study where the viability of selected low-cost optical sensors and optic fiber will be tested in regards to its potential as a sweat monitoring tool, namely to extract compositional and quantified information of certain key components commonly found in sweat, in their respective concentration range. With this study, the author intends to explore new sweat monitoring techniques based on optical measurements. To accomplish this, an array of optical measurement approaches is evaluated for their viability and compared using a synthetic sweat solution as a reference.

To meet this end, a work plan and several milestones were set. The proposed milestones were as follows:

- Literature review of similar technology or sweat studies;
- Acquire knowledge concerning optical physics and its applications;
- Synthesis of a simple artificial sweat solution based on human sweat's parameters
- Analysis of component solution and artificial sweat using 5 commercially available reflectance optical sensors and optical fiber;

- Analysis and characterization of both single compound and artificial sweat solutions in different zones of the electromagnetic spectrum
- Statistical analysis of the acquired database;
- Determining sensor reliability and optimal usage;
- Documentation and thesis writing.

1.4 – Dissertation's achievements

The proposed objectives inevitably tread in uncharted territory regarding sweat monitoring. As such, this dissertation presents several contributions to this topic as a novel approach in the exploration of optical techniques to sweat monitoring.

Firstly, the literature review presented allowed the gathering and understanding of several state-of-the-art sweat monitoring technologies. The scrutinized compilation of electrochemical and colorimetric techniques thoroughly highlights their strengths and weaknesses while showcasing the optical sensor's capabilities in covering the shortcomings of the established techniques to the best of the author's knowledge.

This study also comprises a novel usage of low-cost commercial optical sensors and optical fiber to sweat assessment while simultaneously developing a unique replicable testing method for these sensors using 3D printing technology. Furthermore, a thorough work pipeline was also engineered that was unique to the tested sensors.

Moreover, the spectroscopy results of this study laid the foundation for future investigation of sweat sensors in different regions of the electromagnetic spectrum.

In summary, this dissertation promoted the exploration of optical exclusive techniques to sweat monitoring while simultaneously presenting promising pathways to future exploration of said subject.

1.5 – Document structure

This thesis is organized in 6 different chapters, each comprising a unique theme. The order of the chapters follows a traditional approach to scientific documenting, having a logical continuity between chapters. The next three chapters will cover several theoretical aspects of the biology (sweat) and technology (sensor and signal processing) used in this scientific work as well as a state-of-the-art study that complements the choices of method followed by its implementation, results and finally, discussion containing final remarks and future prospects for the study at hand. Lastly, the bibliography cited throughout the course of the dissertation will be presented for consultation.

A more detailed explanation of the remaining chapter's contents are as follows:

- Chapter 2 – Sweat: Composition and physiological relevance

This chapter covers the basic theoretical notions behind sweat composition and physiology. It is divided into 5 different sections where sweat production, composition, regional distribution

and pathological interactions will be thoroughly covered as well as key component behavior in a dehydration state.

- Chapter 3 – State-of-the-art

This chapter covers some techniques used for sweat analysis in recent years that have a substantial degree of relevancy or relatability to the method suggested in this document. It also covers each technique's strengths and weaknesses allowing for extrapolation regarding the theoretical advantages and disadvantages of the proposed method. It includes 3 sections, addressing different state-of-the-art approaches to sweat monitoring including their strengths and weaknesses.

- Chapter 4 – Optic techniques and operating principals

In this chapter, divided into 4 sections and 5 sub-sections, the physical principles by which optical sensors and fiber operate will be reviewed as well as the theoretical phenomenons inherently associated with optical techniques such as absorbance, reflectance and transmittance. In addition to this, the sensors and the optic fiber used in this study will also be described and characterized individually. Finally, a brief description concerning the wide-spectrum techniques employed (ATR-FTIR and UV-VIS) will be covered.

- Chapter 5 – Methodology

Here, a traditional approach to experiment methodologies is conducted. From compound selection and solution preparation, to experimental setup and statistical analysis, this chapter describes the practical procedures employed and the overarching pipeline of this work.

- Chapter 6 – Results and discussion

The results for the suggested experiments are presented, starting with the wide-range techniques spectrums and concluding with the sensors and optic fiber results. Additionally, a discussion section is presented where the validity and significance of the results are scrutinized to the best of the author's ability.

- Chapter 7 – Conclusion and future work

Lastly, a general overview of the whole study is presented here, encompassing the author's outlook on this work while addressing the established goals.

Furthermore, a section is dedicated to future prospects of this study where the author discusses the project's continuity by highlighting important aspects that need to be addressed in the future.

Chapter 2

Sweat: Composition and physiological relevance

Perspiration is the physiological process exclusive to mammals by which the biological fluid called sweat is produced. This secretion is produced at the skin's level and plays a key role in several aspects of mammalian homeostasis [7]. Starting on its production, this chapter will cover the key aspects to take in consideration when planning to perform a sweat analysis.

2.1 – Sweat gland morphology, histology and sweat production

There are two major sources of heat that can trigger the sweating response: Metabolic heat (heat produced by metabolic pathways such as physical exercise) and External heat (heat of environmental origin) [8]. In both cases, the sensing of said heat is attributed to the specialized central and peripheral neurons called thermoreceptors [9]. Upon the sensing of a certain heat threshold, these neurons fire and send information to the hypothalamus which consequently triggers sweating and vasodilatory responses [10]. The production of sweat is, then, possible due to the presence of epithelial formations in the skin's derme and hypoderm usually called sweat glands. These are divided into two major categories: Eccrine glands and apocrine glands. There is also a third more recent category that is commonly addressed as "mixed sweat gland" as it possesses mixed characteristics from the two major groups. These are called apoeccrine sweat glands [11].

Eccrine and apocrine glands are the most prominent types of sweat glands found in the human body, however, in between these two types, there is a big distribution discrepancy and overall quantity as well as some morphological and physiological differences.

Morphologically, an eccrine gland is comprised of a single tubular structure that has two distinguishable areas: The secretory coil, an epithelial glomeruli found deep within the dermis or the hypodermis, and the duct, a straight epithelial tube that connects the glomeruli to the skin's surface [12]. Even though eccrine gland size can greatly vary between individuals or even within the same organism, these structures tend to measure between three to five millimeters

length-wise and thirty to forty-five micrometers in diameter [13]. Eccrine glands are the most represented type of sweat glands in the human body, a single person may possess from two to five million of these glands scattered throughout the whole body with increased area incidence in certain areas such as the palms and soles where the incidence of these sweat glands can go up to 700 glands per cubic centimeter [14].

Although similar, apocrine glands, are substantially bigger than the former and have a key difference in the overall structure. Instead of having a duct that connects the secretion coil to the skin's surface, the duct on these glands rather connects to a nearby hair follicle which by itself is associated with a sebaceous gland. Its distribution is also very specific and distinct as these sweat glands are only present in the axillae, the pubic and anal regions [7][15].

Physiologically, all sweat glands entail three different cell types that actively intervene in the sweat production and excretion: Clear cells, dark cells and myoepithelial cells. Both clear and dark cells are responsible for sweat secretion. The most relevant difference between them is that dark cells possess many electron-dense granules whereas clear cells do not. Instead, these present a large quantity of mitochondria and membrane villi. Although clear cells carry most of the secretory functions, dark cells are also known today to share that function in addition to the secretion of specific glycoproteins. Finally, myoepithelial cells have three main roles: mechanically support the secretion cells, mechanically excrete sweat by contractile force and promoting regeneration by retaining sweat gland stem cells [12][15]. The present study, however, will focus on the eccrine gland sweat production as past studies have shown that this sweat type is believed to possess the highest representation of relevant biomarkers [16].

2.2 – Sweat composition

For many years, it was believed that sweat was a biological secretion made up of mostly water and several ions that give its salty taste. Although this information is not completely incorrect, nowadays, scientists have scrutinized this biological fluid and have delved deeper into its composition. A study conducted in 2006 by Aleksandr Stefaniak and Christopher Harvey thoroughly described all the components present in human sweat and their respective maximum, minimum and median concentrations [17].

According to this study, the highest represented substances found in sweat (aside from water) are primary electrolytes. Sodium and Chloride are the ones that possess highest quantities, translating to an average representation of 3.1×10^{-2} and 2.3×10^{-2} respectively. Within the primary electrolyte category, Calcium, Potassium and Bicarbonate also have significant representation. However, other biological substances are also well represented here, comprising a wide range of organic molecules such as amino acids, vitamins and even other human secretions like urea [17]. Furthermore, some of these substances such as Glucose, Lactic acid and the previously mentioned urea, are linked with several physiological disorders and can be used as biomarkers to help the screening and diagnosis of certain pathologies. These biomarkers will be thoroughly covered in the next section. Table 1 illustrates all the compounds found by Stefaniak and Harvey and their respective quantities, divided by compound category.

Table 2.1 - Sweat composition reported by Stefaniak and Harvey in 2010 [18].

Constituents[a]	Median concentration (M)	Minimum concentration (M)	Maximum concentration (M)
Primary electrolytes			
Sodium	**3.1×10^{-2}**	**1.1×10^{-4}**	**3.9×10^{-1}**
Chloride	**2.3×10^{-2}**	**1.7×10^{-5}**	**2.8×10^{-1}**
Calcium	5.2×10^{-3}	4.7×10^{-6}	1.5×10^{-2}
Potassium	6.1×10^{-3}	6.7×10^{-6}	3.8×10^{-2}
Magnesium	8.2×10^{-5}	7.4×10^{-8}	3.8×10^{-3}
Phosphate	3.1×10^{-4}	2.3×10^{-5}	1.1×10^{-3}
Bicarbonate	3.0×10^{-3}	2.6×10^{-4}	2.0×10^{-2}
Ionic constituents			
Sulfate	4.2×10^{-4}	7.0×10^{-5}	2.0×10^{-3}
Sulfur	2.3×10^{-3}	2.2×10^{-4}	2.3×10^{-3}
Fluoride	1.1×10^{-5}	5.8×10^{-8}	9.5×10^{-5}
Phosphorous	1.3×10^{-5}	2.2×10^{-8}	1.5×10^{-3}
Bromine	2.3×10^{-6}	4.4×10^{-9}	6.3×10^{-6}
Cadmium	1.8×10^{-8}	1.2×10^{-8}	2.3×10^{-8}
Copper	9.4×10^{-7}	1.3×10^{-8}	1.2×10^{-3}
Iodide	7.1×10^{-8}	7.9×10^{-11}	7.5×10^{-5}
Iron	9.8×10^{-6}	1.5×10^{-8}	1.1×10^{-3}
Lead	1.2×10^{-7}	3.5×10^{-9}	2.0×10^{-7}
Manganese	1.1×10^{-6}	1.1×10^{-9}	1.3×10^{-3}
Nickel	4.2×10^{-7}	1.7×10^{-9}	8.3×10^{-7}
Zinc	1.3×10^{-5}	1.4×10^{-8}	2.3×10^{-5}
Lactic acid	**1.4×10^{-2}**	**3.7×10^{-3}**	**5.0×10^{-2}**
Pyruvic acid	1.8×10^{-4}	1.0×10^{-7}	1.0×10^{-3}
Butyric acid	2.4×10^{-6}	5.0×10^{-7}	6.0×10^{-6}
Acetic acid	1.3×10^{-4}	5.9×10^{-5}	4.2×10^{-4}
Hexanoic acid	9.0×10^{-7}	2.0×10^{-7}	3.5×10^{-6}
Propionic acid	3.5×10^{-6}	1.2×10^{-6}	7.4×10^{-6}
Isobutyric acid	8.0×10^{-7}	NR[b]	2.8×10^{-6}
Isovaleric acid	1.1×10^{-6}	2.0×10^{-7}	4.5×10^{-6}
Glucose	**1.7×10^{-4}**	**5.6×10^{-6}**	**2.2×10^{-3}**
Amino acids			
Alanine	**3.6×10^{-4}**	**NR**	**NR**
Arginine	7.8×10^{-4}	3.3×10^{-4}	4.4×10^{-3}
Aspartic acid	3.4×10^{-4}	NR	NR
Citrulline	4.0×10^{-4}	NR	NR
Glutamic acid	3.7×10^{-4}	NR	NR
Glycine	3.9×10^{-4}	NR	NR
Histidine	5.2×10^{-4}	2.7×10^{-4}	1.3×10^{-2}
Isoleucine	1.7×10^{-4}	7.6×10^{-5}	2.8×10^{-4}
Leucine	2.1×10^{-4}	9.1×10^{-5}	3.2×10^{-4}
Lysine	1.5×10^{-4}	9.6×10^{-5}	2.2×10^{-3}
Ornithine	1.5×10^{-4}	NR	NR
Phenylalanine	1.3×10^{-4}	6.1×10^{-5}	2.1×10^{-4}
Threonine	4.5×10^{-4}	1.4×10^{-4}	7.6×10^{-4}
Tryptophan	5.5×10^{-5}	2.0×10^{-5}	9.1×10^{-5}
Tyrosine	1.7×10^{-4}	6.6×10^{-5}	3.0×10^{-4}
Valine	2.5×10^{-4}	1.3×10^{-4}	3.8×10^{-4}
Ammonia	5.2×10^{-3}	4.7×10^{-4}	2.5×10^{-2}
Uric acid	5.9×10^{-5}	4.2×10^{-6}	4.8×10^{-3}
Urea	**1.0×10^{-2}**	**1.8×10^{-3}**	**4.6×10^{-2}**
Creatinine	8.4×10^{-5}	8.8×10^{-6}	2.0×10^{-3}
Creatine	1.5×10^{-5}	NR	NR
Vitamins			
Thiamine	5.0×10^{-3}	4.5×10^{-9}	5.0×10^{0}
Riboflavin	2.0×10^{-2}	1.3×10^{-8}	8.0×10^{-1}
Nicotinic acid	4.1×10^{-1}	1.4×10^{-7}	3.7×10^{0}
Pantothenic acid	**1.3×10^{-1}**	**6.8×10^{-8}**	**3.6×10^{0}**
Pyridoxine	1.0×10^{-8}	2.4×10^{-9}	5.0×10^{-3}
Folic acid	1.6×10^{-8}	1.2×10^{-8}	2.0×10^{-8}
Ascorbic acid	1.0×10^{-5}	1.1×10^{-7}	3.6×10^{-5}
Dehydroascorbic acid	1.1×10^{-5}	7.6×10^{-9}	8.6×10^{-4}
Inositol	1.6×10^{-6}	8.3×10^{-7}	1.2×10^{0}
Choline	2.6×10^{-5}	6.8×10^{-7}	1.5×10^{-4}
p-Aminobenzoic acid	7.1×10^{-8}	5.8×10^{-9}	1.8×10^{-2}

[a]Constituents in bold fonts were indicator constituents monitored in this study to evaluate chemical stability of the sweat solvent. [b] NR = not reported in literature

Four years later, a study conducted by the same scientists built upon their previous knowledge foundation about sweat and proposed a chemical formulation for producing artificial human sweat and its respective handling and storing protocols [18]. Although replicable and trustworthy, Harvey's formulation is quite complex as it is comprised of 60 different compounds, some of which are very expensive and represented in minuscule quantities. The present study intends to follow up on this formulation by finding a middle ground, developing a cheap but reliable alternative to actual human sweat for testing purposes.

2.3 – Sweat as a physiological indicator

Historical records dating from the Renaissance period associate the salty taste of the skin with bad omens or even imminent death. In this period of history, there was still a strong belief in the occult and many pathological symptoms were still correlated with "hexes" and "witch-craft". In 1606, reports from a Spanish medicine professor stated that "the fingers taste salty after rubbing the forehead of the bewitched child" [19][20]. Even back then, the simple salinity cue that could be experienced by anyone already served as a somewhat reliable source of information regarding the wellbeing of an individual. This salty taste that was described in these ancient documents refers to the well-known fluid that we know today as sweat and since then, science and medicine discovered novel and stronger correlations of this substance with other pathologies and conditions.

Cystic fibrosis, a well-documented genetic disorder is a pathology characterized by the modification of several epithelial tissues such as the lungs, the pancreas and the skin. Its origin can be recessive homozygous and at the skin level, this mutation hinders the reabsorption of NaCl in the sweat ducts [21]. This results in a significant increase of NaCl concentration in the sweat in homozygous individuals. Research has also shown that heterozygotic individuals can be diagnosed with cystic fibrosis but the physiological trend presented above does not prevail in these cases [13]. Given this, the gold standard in the screening of this disease is still to this day, the sweat chloride test which is a chemical test that measures the Cl^- concentration in the individual sweat and compares it against standard values [22]. Furthermore, the interest in the salinity of the sweat is not limited to the diagnosis of cystic fibrosis as it also presents an important cue for determining the dehydration state of an individual [3].

Lactic acid, another substance that can be found in human sweat, is also an important biomarker that has been studied thoroughly. For many years, medicine was able to successfully establish a relation between the concentration of lactic acid in the blood and intense physical activity [23], [24]. Depending on the intensity of the physical exercise, the O_2 intake from the individual might not be enough to satisfy the active muscle's needs. In these cases, the muscle itself seeks other ways of producing ATP. In this scenario, in addition to the aerobic respiration, muscle cells perform anaerobic respiration which is a glycolytic pathway that does not require the presence of O^2 and that results in the formation and accumulation of lactic acid in the muscle. The lactic acid buildup in the muscles can be harmful and toxic so the body has several

ways of excreting the excess Lactate [25], [26]. Transporting this excess through the bloodstream to the main secretory organs is a well-known physiological response and hence the correlations mentioned above, However, the available methods to analyse the lactate from a subject are invasive processes that are not practical and the extraction of it can potentially expose the individual to infections.

Other studies focused on the issue described and prospected parallel concentration trends in human sweat, similarly to what was known in the blood. These studies successfully traced a similar correlation between sweat's and blood's concentration upon intensive physical activity [27], [28]. These findings led to the development of experimental systems for tracking exercise intensity by lactic acid concentration in sweat [29]. This system will be further analyzed in Chapter 4.

Glucose is also a very relevant biological compound as it is the base component for the functioning of both the aforementioned glycolytic pathways (aerobic and anaerobic). Diabetes is a very common disease (in 2015, 9,4% of the United States of America population had been diagnosed with diabetes) that interferes directly with these pathways, especially type II which is the most representative variant comprising 90 to 95% of the diabetes incidences in the United States of America [30]. This variant consists on the inability of the patient's body to produce enough and/or correctly use insulin which is a hormone peptide responsible by the lysis (breakage) of many sugar's chemical bonds. The monitoring of glucose in these patients is crucial and is still, nowadays, done by an invasive sampling of the patient's blood, being impractical, painful and prone to infections. Several studies aimed at finding alternatives to this system and led to the discovery of correlations between glucose levels found in blood and glucose levels found in sweat [31], [32]. This path proved to be promising and many developers now look to the development of systems that can integrate this relation to measure glucose levels in diabetes patients through the non-invasive analysis of the patient's sweat [33], [34].

Other studies address these novel glucose measurement methods as potential tools to predict and prevent hypoglycemic shock occurrences during intensive exercise activities [35]. These novelties will also be discussed later.

Urea is yet another biological secretion which can be found in human sweat. It is most commonly associated with the urinary system, being one of the main components of this system's excretions: urine. In the same fashion, however, studies have also aimed at determining the relevancy of the presence of urea in sweat and its oscillations. Scientists believe that the quantities of urea found in the human sweat can be of medical relevance for healthcare monitoring [36], [37].

2.4 – Sweat rates and Regional variability

The physiology behind the human thermoregulatory processes is very complex as it entails many variables from sweat gland type and density to the individual intraspecificity. The rating of sweat is a prime example of this complexity as it is one of the most affected and variable parameters in the sweating response. Sweat rates vary greatly with the type, intensity and duration of physical exercise as well with acclimatization processes. Furthermore, one of the most impactful variables in this domain is the regional disposition of the sweat glands. Studies have shown that certain anatomical sites have greater sweat rates than others and that the variability between these localized sites can reach variations of 360% [2]. Medical conditions such as hypohidrosis and hyperhidrosis can also drastically alter an individual's sweating rate [38], [39].

2.5 – Summary

Sweat is a biological secretion that can be easily sampled without using invasive means. This is possible thanks to the large amounts of eccrine sweat glands distributed throughout the whole body. This secretion is also very rich in its composition comprising a variety of electrolytes and organic molecules that are nowadays well described and quantified. Furthermore, many of these components have proven to be crucial factors in the diagnosis of certain pathologies or actively aiding in the monitoring and understanding of an individual's health.

Chapter 3

State-of-the-art

Upon the realization of sweat's potential as a physiological indicator comes the growing interest in its analysis and sampling techniques. Moreover, in the current era, measuring is not enough as medicine comes closer to personal monitoring systems that are wearable, accurate and cheap [33].

Statistics show that interest in this particular field has skyrocketed as scientific document publications containing both the keywords: "sweat" and "sensor" have seen a massive surge from 2015 onwards.

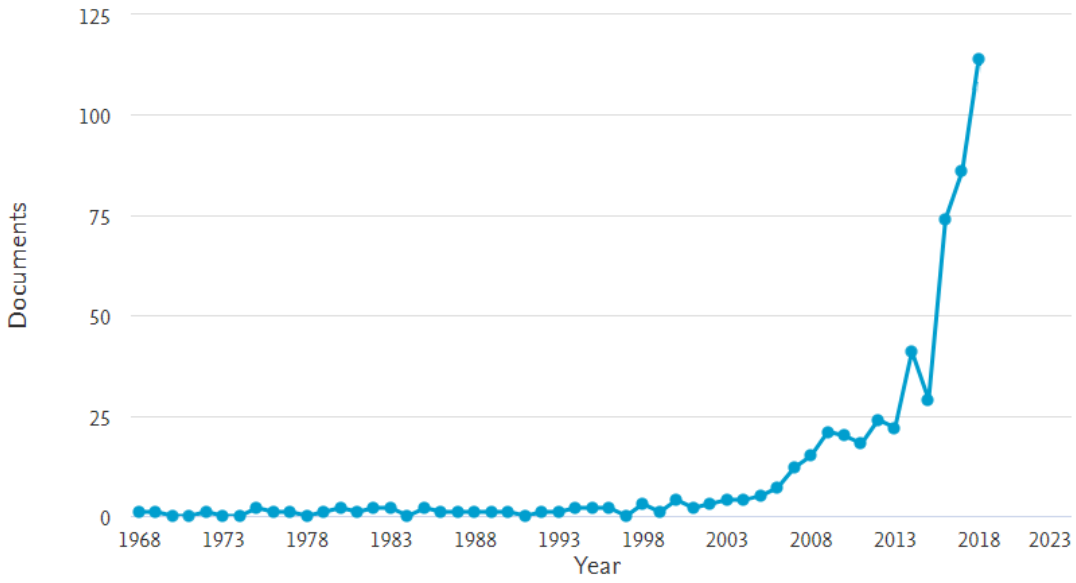

Figure 3.1 – Statistical data for the keywords "sweat" and "sensor" from the Scopus database.

Figure 4.1 shows a chart comparing the number of publications containing the selected keywords per year from 1968 to 2018, year which this number peaked with 114 publications comprising the words “sweat” and “sensor”.

This chapter will be dedicated to what recent studies have achieved regarding the analysis of sweat using several different technologies. Colorimetric and electrochemical techniques will be reviewed as well as their target measurand. Furthermore, the enclosure of optical techniques in this type of analysis will be discussed as well as the innovative aspects of this work that intend to build upon the foundation laid by the existing approaches.

3.1 – Colorimetric techniques

There are already several published works that use colorimetric approaches to sweat analysis, however, these approaches have different target measurands and overall operating principles.

In 2009, Morris et al. [5] developed a “Bio-sensing textile based patch” that encompassed a colorimetric approach to sweat analysis. In this work, the textile patch contained a gathering structure that would conduct the collected sweat into a pH-sensitive dye. Depending on the sweat’s pH, the dye would react and change colour. An incorporated optical sensor comprised of emitter-detector LEDs will then detect the pH sensor’s colour and transmit it wirelessly to a laptop. Despite being efficient, this work is limited to the sweat’s pH analysis which is a very general parameter to evaluate since changes in pH are not limited to the concentration of primary electrolytes but may also be heavy influenced by other sweat components such as lactic acid [40].

Regarding these, novel approaches aimed at making these measurements more specific. A patent registered in 2018 by Rao Ashwin et al. [33] covered a non-invasive colorimetric sensor aimed ate detecting glucose levels in sweat. In this patent, a more complex patch was developed that simultaneously encompassed a Hydrocromic (wetness indicator), pH and a glucose sensor in the same patch. Despite not having any electrical support to the sensor, this glucose sensor is far more sophisticated as it operates by using specific enzymes that interact with glucose such as glucose oxidase. The complex formed from this interaction reacts further with a chromogen that makes the sample change colour depending on the concentration. This reaction can be visually checked at any time and compared against control colours that are connected to certain key concentrations. Although accurate and cheap, this invention faces the problem of containing an irreversible reaction that limits monitoring times and intervals.

Similarly, in 2014, Huang Xian et al. [41] developed a wearable patch that used colorimetry to measure the pH and concentration of primary electrolytes in sweat. This model, however, had the addition of a volumetric technique that allowed to measure the volume of the collected sweat sample.

Conversely, a 2013 study by Sakaguchi Kazuhiko et al. [32] developed a wearable system that combined colorimetric and electrochemical techniques. In this work, there were both glucose and sodium sensory mechanisms. The glucose system operated by the reaction of 4 different enzymes with the glucose found in sweat [42]. The formed complex would then react with a fluorochrome compound and was later evaluated using a fluorescence plate reader. The sodium concentration, on the other hand, was analysed using a sodium-selective electrode. This

study illustrates the problem of the simultaneous measuring of different factors that often require independent methodologies as described.

3.2 – Electrochemical techniques

There are also reports of exclusively electrochemical approaches to sweat monitorization. A study by Enomoto et al. in 2017 [29], proposed a method of monitoring the concentration of lactic acid in human sweat and used it to register its variability during physical exercise to assess its intensity. In this study, the biosensor used detects lactic acid by the reaction of the lactic acid with lactate oxidase which results in the production of a component called hydrogen peroxide [43]. This reaction is traduced into electrical current values and so a correlation between the oxidized lactic acid and the current values is established showing a sensitivity of 0,196 μA/mM. Furthermore, this sensor proved to have a high selectivity index which means other sweat compounds cannot interfere with the measurements. Moreover, this system introduced a novel flow injection system using phosphate buffer saline to improve stabilization of baseline values as these proved to be quite unstable.

On the same year, Hyunjae Lee et al. [34] published a parallel work, addressing glucose monitoring instead of the lactic acid. However, this work presented several advancements in comparison to the former. It introduced a multimodal approach to glucose monitoring using different electrochemical sensors to this end. It comprised of 4 sensors: One temperature sensor that operates by resistors, one humidity sensor that operates by impedance, one enzyme-based glucose sensor whose operability aligns with the methods described in the previous section, one glucose sensor called “Prussian blue-deposited porous gold electrode”, which is a deposition technique for nanocomposite films triggered by the redox reaction on gold nanoparticles [44]. The glucose response is modulated by the interaction of these four sensors producing much more accurate and sensitive readings. In addition to this, this system also includes a drug delivery device that operates based on the multimodal sensor's response. Although revolutionary, this work solely focusses on one of the sweat’s components which raises the issue regarding the single dimensionality of the measurement which still hinders the sweat’s biomarker potential.

A 2014 study by Bandodkar Amay J. et al. [45] introduced the concept of a sweat sensory system that could double as a fashion accessory in the form of a tattoo. This work led a potentiometric approach to sodium concentration measurement by using an ion selective electrode. This system operates by measuring the difference between the reference electrode charge and the electric potential generated by the specified ion, in this case, sodium. This type of behavior was firstly reported on the functionality of the galvanic cell [46], [47]. This system was then linked with a wearable transceiver that would send, in real-time, the sensor’s information wirelessly. The results of this work showed a clear correlation between the potentiometric readings with periods of physical exercise.

In the same fashion, a more recent work by Arnaud Cazalé et al. in 2016 [48], presented a similar approach to sodium monitoring, however, this work not only included the use of the already described ion specific electrode but also included a different potentiometric approach

to sodium monitoring, an ion-sensitive field-effect transistor. This technology operates based on the change in the current across the transistor which varies according to the sensed ion concentration which in this study was sodium. These biosensors were able to be very sensitive to sodium concentration changes due to silver-based electrodes used for referencing. Furthermore, this study was able to establish a linear correlation between the sodium concentration in sweat and its anion counterpart, chloride, which further validated the accuracy of these sensors. In addition to this, a passive sweat pump was also developed to regulate the sweat's flow and interaction with the sensors.

Despite their validation and reliability, the electrolyte approach conducted by both these studies is still narrow as it is limited to the factors that can be measured with its current setup.

Finally, a study by Liu Gengchen et al. in 2016 [49] used yet a different method to characterize sweat's conductivity. This study was carried without focusing on a single measurand unlike the previous ones but instead focusing solely on discriminating sweat's conductivity by electrochemical impedance spectroscopy. This bio-sensor operated on the principle that different ionic concentrations in sweat would create different currents when an external voltage source was applied to the system. This system also involved a wearable bracelet with a built-in sweat collector and a wireless transceiver. The results of this study showed promising correlations between the sweat's conductivity and physical exercise from in-vivo testing. However, as the first reviewed article, this study addresses only a single parameter that is very general and therefore less relevant for diagnostic.

3.3 – Bridging optical sensors into sweat monitoring

The presented cases illustrate the success of several systems in identifying different sweat compounds. Several measurands were addressed as well as different approaches to electrochemical and colorimetric techniques. However, with this analysis, some issues were raised regarding the said techniques. Firstly, most of the works reviewed only addressed a single sweat characteristic, being an electrolyte or an organic molecule such as glucose or lactic acid. Being very specific and accurate, versatility is lost in these models as changing the setups required for other analysis requires independent methodologies. The colorimetric and some electrochemical techniques rely heavily on compounds whose reactions are irreversible (i.e. dyes and lactic acid oxidation) and therefore limiting the monitoring time that a given system can be used for, before the sensor saturates or before the compound reserve is depleted.

Another aspect that was absent from almost every case presented is the use of optical measurement techniques. Morris work [5] did actually incorporate an optical sensor in his pH sweat sensor patch, however, the referred optical sensor served only as a support sensory technique to convey information since the main sensory aspect of the pH relied solely on the colorimetric pH band incorporated in the patch that would change colour according to the sweat's pH. Apart from this supporting role, the author of this document could not find any optical focused techniques for sweat monitoring. However, there are some sweat unrelated studies that employ purely optical approaches to simple glucose solutions.

A study by Haxha Shyqyri and Jhoja Jaspreet in 2016 [50] aimed at developing a non-invasive method of determining glucose levels in blood by using NIR spectroscopy to estimate glucose levels based on the transmittance of a NIR beam that would travel through the patient's finger as it does through an aqueous solution in regular spectroscopy machinery. This was tested in-vitro against known glucose concentrations and in-vivo against other medically implemented methods both with promising results. The in-vitro results presented a very good separability factor and followed the expected trend. The in-vivo results also followed the standard equipment measures trend with a significant degree of likelihood. This study validated the usage of optical NIR techniques to detect and quantify glucose both in solution and in a live patient. Being glucose one of the many key components in sweat monitoring, the inclusion of a similar optical technique for sweat monitoring holds a significant experimentation value. However, a spectrometric approach relies on very powerful spectrometry tools that are both very expensive and unpractical.

In 1994, Takashi Takeo and Hajime Hattori developed an optical fiber probe to test whether this optical technique was useful to estimate the dehydration state of the skin [51]. This probe was built by removing a portion of the cladding from the optic fiber that would then be in contact with the skin. They stated that it would be expected to find bigger hydration values near the basal layer of the skin. By using a stripping technique, they observed the optical loss through consecutive strippings of the outer skin layer and then compared these results with an electrical conductance technique. The results of this study revealed that the lower skin layers were, in fact, more hydrated and that the optical fiber probe could measure these differences accurately since it followed the pattern observed on the conductance test.

Another similar study was published in 2009 by Binu S. [4] which comprised of the determination of different glucose concentrations in aqueous solution by Fibre optic methodology. In this work, the fiber optic was used to sense variations of the refractive index of glucose solutions with differing concentrations. The results provided show that the refractive index of the solution is directly proportional to glucose's density and concentration. Despite the sensor's high sensitivity, the most attractive feature in this study is the simplistic and low-cost build that can easily replicable and introduced in several industries.

Upon taking on these recent approaches to sweat monitoring, there is a striking lack of optical studies developed around this subject. Hopefully, parallel optical methodologies have been developed and tested on important bio-molecules [4], [50]. This way, the author of this work intends to bridge these two concepts (sweat monitoring and optical techniques) to develop a gateway to new optical methodologies applied in sweat characterization and at the same time to provide reliable, versatile and low-cost sensory options that can be used to measure one or more key sweat biomarkers.

Chapter 4

Optic techniques and operating principals

The studies of Shyqyri and Binu have shed some light on the optical sensor's potential in measuring glucose concentrations [4], [50]. The present work focuses on a more extensive approach as it aims to analyze the behavior of multiple biomarkers using optical techniques. In this preliminary study, Glucose and NaCl concentrations were selected as test biomarkers due to their recurring interest in most of the covered studies.

The aim of this preliminary work is to find the most sensible and accurate sensors for different concentrations of the referred bio-markers. Thus, several commercially available optic sensors were bought covering a wide range of wavelengths to determine the optimal wavelength for each biomarker detection and quantification.

The used sensors operate by emitting and detecting electromagnetic waves centered at defined fixed wavelengths. Thus, allowing to evaluate the sample under analysis at different portions of the electromagnetic spectrum. This chapter will cover the basic principles of reflectance spectroscopy and optic fiber as well as their associated phenomenons such as reflectance, absorbance, transmittance and scattering. Furthermore, each sensor will be described individually regarding its features and interface.

4.1 – Principles of reflectance

Spectroscopy is a field of physics that studies the interactions between electromagnetic radiation and atoms or molecules. These interactions are conveyed by different phenomenons regarding emission, absorption and scattering of electromagnetic waves [52].

Reflectance spectroscopy is a component of spectroscopy that focuses on the study of electromagnetic waves as a relation between its wavelength and the amount of radiation (in this case, photons) that is reflected and scattered from a given medium.

However, this phenomenon is not an independent instance as it is directly influenced and correlated to the absorbed radiation. Materials, liquids, solutions or gases have an absorption coefficient based on its chemical composition and conformation.

When photons collide with the surface of an atom, they can either be absorbed or scattered. Absorption can be caused through electronic or vibrational processes and the absorptive behavior is well characterized by the Beer-Lambert law which quantifies the transmitted and absorbed light by comparing the intensity of the light before and after passing through the medium as a function of wavelength. According to this law, the absorbance of light increases with solution concentration and grain size as the internal path size is proportional to its grain counterpart [53], [54].

The scattering process, on the other hand, happens when light is not totally absorbed and causes photons to be reflected. Unlike a perfect mirror, when light is scattered on an irregular surface such as a chemical solution, the reflectivity angles greatly vary causing an uneven distribution of photons in several directions. This type of reflection is known as diffuse reflection. A special case of scattering can be verified when the reflectivity angle of a given photon is 180º which means that the photon is directly reflected back at its source. This type of scattering is sometimes called backscattering and it is the key mechanism behind the acquired optical sensor's functionality [55], [56].

In 1984, Roger Clark and Ted Roush demonstrated that the reflectance of a component was inversely proportional to its grain size using the mentioned relations from the beer-lambert law [57]. For the same concentration, smaller grain particles have an increased surface/volume ratio which boosts its reflectance. Conversely, bigger particles have a lower surface/volume ratio and, according to beer-lambert's law, are also more absorptive which overall reduces its reflectance [53].

These findings validate the usage of reflectance spectroscopy to compare different components and different component concentrations.

4.2 – Reflectance Optic Sensors

This section will be dedicated to covering each sensor's features and specifications. All the sensors have the same base functionality: They consist of an electronic chip containing one or more light emitters and a photosensitive cell. They are designed to emit light at a certain intensity and wavelength interval which will be reflected on the target medium and received on the correspondent photosensitive cell. Thus, they are reflectance sensors and therefore obey the principles described above. Since the final objective of the study is to develop a system that can monitor human sweat, the wavelengths selected for the study were conditioned to a range that is not harmful for human exposure. The range comprises wavelengths from 450 nm to 940 nm.

Data collection and sensory control were developed in MATLAB by INESC-TEC's BRAIN group research associates where a comprehensive GUI allowed users to select the desired sensor to measure, as well as its corresponding connection port and number of measures carried out in a

single sample. This method was applied to all sensors except one: VCNL4020. This specific interface will be thoroughly covered on the sensor's designated sub-section.

4.2.1 – Visible spectroscopy sensor

Developed by AMS, AS7262 is a 6-channel visible spectroscopy sensor with a built-in temperature sensor. Each channel contains a different wavelength on the visible light spectrum: 450nm, 500nm, 550nm, 570nm, 600nm and 650nm, each possessing a 40nm FWHM. It features a photosensitive panel and emission LED with an adjustable current system that can vary from 12.5 to 100 mA. It also already has a built-in 16-bit ADC which eliminates the need to sample the sensor's signal. The whole system is imbued in a 20-pin LGA package with the dimensions 4.5mm x 4.7mm x 2.5mm and operates at low power which allows for extensive use with a relatively small battery. Does not require calibration and is minimally affected by temperature drifts and usage.

Data access and sensor control can be implemented using an I^2C interface device, for this study, an Arduino Uno was used to this effect [58].

The computer interface used was the previously described GUI in MATLAB. For the measurement of this specific sensor, readings from all the 6 channels were simultaneously recorded in each instance as well as its corresponding temperature.

4.2.2 – NIR spectroscopy sensor

Also developed by AMS, AS7263's features are similar to the former with the exception of its range wavelengths. It is instead a NIR spectral sensor and so it has 6 NIR channels comprising the following wavelengths: 610nm, 680nm, 730nm, 760nm, 810nm and 860nm. In this case, each channel possesses 20nm FWHM instead of the 40nm of the former version [59].

Control and data bridging was also done using an Arduino Uno.

Using the same MATLAB GUI, sensory information was also read from all 6 channels simultaneously however, for this sensor, temperature information was not retrieved.

4.2.3 – Photoplethysmography sensor

MAX30101 is a Pulse Oximeter and Heart-Rate Sensor developed by Maxim Integrated. Despite being a multi-purpose biomedical device, for the inclusion of this study, only part of its functionality is going to be addressed. It features a photosensitive cell and 3 internal current customizable LEDs, each corresponding to different wavelength emissions: 537nm (green) with 35nm FWHM, 660nm (red) with 20nm FWHM and 880nm (IR) with 30nm FWHM. It also features an 18-Bit ADC with an ambient light cancellation system and a digital noise remover that ensures a high SNR. It operates on low power and has 2 power supplies: a 1.8V power supply for the chip and a separate 4.5V supply for the internal LEDs. The whole system is encompassed in a 14-pin optical module with the following dimensions: 5.6mm x 3.3mm x 1.55mm [60].

Instead of an Arduino, this system is mounted on the MAX30101 Evaluation System, a Kit developed and commercialized as well by Maxim Integrated and comprises a USBOSMB

motherboard that enables a USB connection to a computer and a MAX30101DBEVKIT which is a daughter board where the sensor is mounted [61].

As such, the bridging of data and sensor control is also carried out by USBOSMB following standard I^2C protocol.

Finally, the previously mentioned MATLAB GUI also serves as the sensors interface for measuring where the user can make measurements using all the available internal LEDs simultaneously.

4.2.4 – Long distance IR sensor

The VL53L1X is a long-distance IR sensor developed by STMicroelectronics which incorporates a novel system (also by the same company) called Time-of-Flight. This system is based on the ST's FlightSense technology which consists in measuring the distance to a target object or surface by not only signal strength (which is dependent on the material's innate reflectivity) but also by quantifying the time interval between the emission and reception of the reflected signal. Unlike the previously described sensors, the VL53L1X features a single IR laser of 940nm and a SPAD light receiver with a built-in lens. It also incorporates an adjustable field-of-view for a specific ROI analysis on the light receiver. It runs on a single low power supply and is integrated on a 12-pin Optical LGA with the following dimensions: 4.9mm x 2.5mm x 1.56mm [62].

It operates on an I^2C interface similar to the previous sensors but this one is capable of working at full speed (400Mhz) and is connected to an Arduino Mega instead of a regular Arduino.

Data collection and device control are also executed through the mentioned MATLAB GUI interface and in addition to reflectivity rates, this system also measures distance to the target.

4.2.5 – Proximity light sensor

Lastly, developed by Vishay Semiconductors, VCNL4020 is a proximity and ambient light sensor. It fully integrates 3 different Vishay diode emitters into a single chip. It features the VLMTG1300-GS08 "True Green" emitter LED which operates at 525nm, the VSMD66694 Dual color emitting diodes which are two emitter LEDs that operate at 660nm (red) and 940nm (classified by the manufacturer as external IR) and the VSMF2890GX01 Infrared diode which operates at 890nm (classified by the manufacturer as Internal IR). It also features a photosensitive receiver, a built-in signal conditioning system a 16-bit ADC converter and an ambient light suppressor. Furthermore, the LED driver current is programmable ranging from 10mA to 200mA in 10mA stages. The VCNL4020 runs on two variable low voltage sources (2.5 to 3.6V for positive supply and 2.5 to 5V for IR anode) and is integrated in a surface-mount board with the following dimensions: 4.90mm x 2.40mm x 0.83mm [63]–[66].

The interface of this sensor is mediated by standard I^2C communication using the SensorXplorer board which is a board also developed by Vishay and that acts as an interface between the sensor and a computer.

In this case, data collection and sensor control were executed in Vishay's signature windows application. This application included a sophisticated GUI that allowed the individual selection of each wavelength and current settings for testing. Furthermore, the software is capable of

tracing real-time graphs of the current sensor's reading and provide some real-time statistical data such as mean and standard deviation [67].

4.3 – Optical Fiber

Optical fiber is a technology that allows the transmission and conduction of electromagnetic waves at a very high speed through very long distances with minimal signal loss by a very thin, flexible fiber. It was initially used in the late 19th century as a medical device to help illuminate hard to reach places in the body, such as internal cavities. Nowadays, it is a wide-spread technology in the communications sector due to its long range and speed properties. The concept of light conduction through a given medium was first documented in the early 1840s by Daniel Colladon and Jacques Babinet in France. They demonstrated two key operating principles of optical fiber by shining a beam of light through a water fountain which conducted light all the way through the water's course. These principles are known today as Refraction and Total internal reflection (TIR) [68].
Refraction is a phenomenon referring to the change in direction of a wave travelling from a given medium to another. The quantification of refraction depends on wave speed difference between mediums and on the direction of the wave itself. For light related phenomenons, this relation is expressed by the Snell's Law which originates the concept of Refractive Index.

$$\frac{\boldsymbol{sin\theta_2}}{\boldsymbol{sin\theta_1}} = \frac{\boldsymbol{v_2}}{\boldsymbol{v_1}} = \frac{\boldsymbol{n_1}}{\boldsymbol{n_2}} \tag{4.1}$$

The Snell's law establishes equivalency between the ratios of the sines of the angles of incidence and refraction (sin02 and sin01), the phase velocities in both mediums (v2/v1) and the inverted indexes of refraction (n1/n2) This dimensionless number describes the speed of propagation of light in a given medium and can be determined by the following equation:

$$\boldsymbol{n} = \frac{\boldsymbol{c}}{\boldsymbol{v}} \tag{4.2}$$

Here, the refractive index (n) is a function of lightspeed in vacuum (c) by the phase velocity of light in the given medium (v) [69].

The refraction phenomenon is usually accompanied by partial reflection of the wave. TIR is a refraction related phenomenon that occurs when an electromagnetic wave reaches the boundary between two mediums at a very steep angle. If the angle exceeds a certain angle value (called critical angle) the wave is completely reflected back to the medium. The range of angles that satisfy this condition is usually denominated acceptance cone and its dimension is dependent on the refractive index's differences between the internal and external medium [68].

Optical fiber has two main components: the core and the cladding. The fiber's core is the internal medium where the electromagnetic waves are enclosured and its usually made out of silica. The cladding is the external layer of the optical fiber which has a slightly different refractive index from the core to facilitate the TIR phenomenon. It is also usually made from

silica. Other protective layers may be present in industrial grade optical fibers, but these do not influence its functionality.

There are two main optical fiber types: Multi-mode fiber and Single-mode fiber. The distinction between these types is located in the fiber's core diameter. Multi-mode fibers have a core diameter larger than 10 micrometers which promotes a greater acceptance cone. This means that more waves can be conducted by the fiber however, this brings the imminent rise of dispersion factors since the bigger acceptance cone implies an increase in path length differences which results in different delivery times of the information. These are usually cheaper but have considerably more losses over their counterparts.

Conversely, single-mode fibers have smaller diameter cores (not exceeding 10 micrometers) which results in a very small acceptance cone, in fact, so small that only accepts a single mode, hence its name. The single path that electromagnetic waves can take ensures the conservation of information over long distances and so it is usually employed in long distance communication. The finer build of these fibers also makes them more expensive than the Multi-mode fibers [69].

4.3.1 – Optical fiber specifications

For this study, a single-mode optical fiber system was assembled in laboratory. The fiber was connected to a laser diode emitter (980nm) and receiver by a specialized fiber connector which was then fixated on an experimental stand where the fiber tip could be inserted directly into the sample. The receiver was then connected to a computer by I2C protocol and the signal was then acquired using the software LABVIEW and the data stored in excel sheets. The emitted laser signal can be transmitted with or without modulation. The laser signal can be modulated in amplitude with a sinusoid function spanning from 1 to 200 Hz.

4.4 – Wide-range techniques

4.4.1 – ATR-FTIR

FTIR is a well-known vibrational spectroscopy technique that operates by identifying and quantifying the absorptive properties of chemical bonds by vibrational processes triggered by different frequencies of infrared light. The quantification of this phenomenon is performed by a built-in interferometer which splits and recombines the IR beam and produces a signal based on the difference between the different beam paths. Finally, this signal is decoded by a Fourier Transformation and the spectrum for the given sample is generated [70].
ATR-FTIR is the application of this spectroscopy technique to a reflectance sampling method called ATR. This sampling technique uses a crystal with a high refractive index (usually diamond or beryllium) which allows the production of evanescent waves. A typical ATR-FTIR setup has the test sample placed over the ATR-FTIR detector directly in contact with the ATR crystal and the IR emitter underneath the crystal at a specific angle. The IR beam starts by entering the ATR crystal where multiple TIR phenomenons take place and several evanescent waves are produced at the border between the crystal and the sample's surface. The beam is then

received when exiting the ATR crystal and the signal differences caused by the evanescent waves are analyzed following the described FTIR procedure [71].

4.4.2 – UV-VIS Absorbance Spectroscopy

UV-VIS is a spectroscopy technique directed at the UV and visible spectrum. It operates on the principle of absorbance and transmission. When photons collide with matter, they can excite bonding and non-bonding electrons to higher energy states by absorbing the photon's energy [72]. The UV-VIS technique uses this phenomenon to quantify the amount of light that has been absorbed or, inversely, transmitted through the sample. To achieve this, a Spectrophotometer is composed of a light source, usually a Halogen or Xenon lamp, from which a single beam of light is filtered using a dispersion device such as a prism so that the machine can run an absorbance analysis through all the lamp's admitted wavelengths. The light beams at different wavelengths pass through a test cell containing the sample to be analyzed and finally detected by a photoelectric cell which converts the light into electrical current. The quantification of the absorbance/transmittance is calculated through the current differences of the emitted and the detected light and is performed following the Beer-Lambert law [73].

$$\boldsymbol{A = \varepsilon * l * c} \tag{4.3}$$

This equation states that the Absorbance (A) of a given solution is equal to its extinction coefficient (ε) times its concentration (c) times the length of the path that the light travels in the solution (l). The solution's absorbance can also be directly calculated from its transmittance (T) by the following equation:

$$\boldsymbol{A = -logT} \tag{4.4}$$

Where the transmittance is initially calculated by the spectrophotometer following:

$$\boldsymbol{T = \frac{I}{I_0}} \tag{4.5}$$

Here the Transmittance is determined by the ratio between the emitted light intensity (I) and received light intensity (I_0) which can be converted into Absorbance [74].

4.5 – Summary

In this chapter, the physical principles behind reflectance sensor functionality were addressed as well as the recurring phenomenons in reflectance spectroscopy such as backscattering. A clear relation between reflectance and particle size was also expressed, which may grant valuable insight on the experience's results.

Furthermore, several commercial sensors were discussed as well as their features and particularities. The wavelengths of each sensor were described comprising a considerable spectrum of visible and NIR light to allow a broad analysis of the selected biomarkers.

Chapter 5

Methodology

To assess the viability of the usage of optical techniques to sweat monitoring, a pipeline of methods was established, and an experimental procedure was laid out. In order to explore and validate this hypothesis, several experimental tests were conducted. From component selection to the development of a controlled and replicable environment for the acquired sensors to the characterization of the spectral tests conducted, this chapter will address, in depth, each of the experimental steps in their respective chronological order covering the technical aspects of the procedures as well as machinery and compound identification. This chapter is divided into 3 major sections and a summary, covering the component's selection, the spectral analysis, and the sensors and optic fiber measurements.

5.1 – Component selection and solution preparation

The goal of this study is to validate the usability of optical techniques to sweat monitoring, however, as shown on chapter 2, sweat is a very unpredictably variable solution as its constitution can be greatly influenced by a panoply of factors even within the same individual. As such, it presents a considerable hurdle to testing new hypothesis as it can introduce many uncontrollable variables in the study. Considering this, one of the key proposals of this study states the synthesis of a sweat substitute solution that is stable and can be replicated in laboratory. To fulfill this purpose, the sweat's compositional data from Harvey and Stefaniak's description was scrutinized and 3 of the most concentrated and representative biomarkers were selected for testing and for the synthesis of the custom artificial sweat solution. The selected components were sodium chloride, urea and lactic acid. Not only they can provide meaningful information about the physiological state of an individual, they're also among the most concentrated compounds found in human sweat.

The concentrations of the selected biomarkers were determined by the maximum concentration values of each biomarker found in sweat [17]. From these concentrations, individual compound solutions and mixtures were created being that every solution was made with deionized water.

Sodium chloride's chemical formulation is NaCl and has a molecular weight of 58.44 g/mol. This single compound solution had a $3.9*10^{-1}$M NaCl (99.5%, PANREAC (lot: A0323804)).

Urea's chemical formulation is CH_4N_2O and has a molecular weight of 60.06 g/mol. This single compound solution had a $4.6*10^{-2}$M CH_4N_2O (99.5%, ACROS-Organics (lot:0000789273)).

Finally, the Lactic Acid chemical formulation is $C_3H_6O_3$ and has a molecular weight of 90.08 g/mol. This single compound solution had a $5.0*10^{-2}$M $C_3H_6O_3$ (90%, VWR Chemicals (lot:17L284005)).

The synthesis of the artificial sweat formulation was done using these three components in the described concentrations and an additional artificial sweat solution was developed using both the medium and maximum concentration values of the same biomarkers found in sweat [18]. This formulation was prepared with **deionized** water and individual solutions of sodium chloride, urea and lactic acid with concentrations of $3.1*10^{-2}$, $1.8*10^{-3}$ and $3.7*10^{-3}$ respectively for the medium and $3.9*10^{-1}$M, $4.6*10^{-2}$M and $5.0*10^{-2}$M respectively for the maximum.

5.2 – Spectral Methodology

With the prepared solutions, two major groups of tests were performed: Spectral analysis using two well-known wide-spectrum techniques (UV-VIS and ATR-FTIR) and commercial sensor and optical fiber testing.

The visible spectrum analysis was performed using a Lambda 35 UV-VIS Spectrometer made by PerkinElmer. Its spectral range is between 190nm and 1100nm and uses a Hamamatsu S1227-66BQ detector. The spectral analysis was conducted between 400nm and 900nm with a resolution of 1nm. The baseline calibration for this device was done using deionized water. In each measurement, 80µl of the sample were pipetted into a quartz cell that was then placed in the Spectrometer. The cell was thoroughly cleaned before and between measurements and the process was repeated 4 times.

The IR spectrum analysis was performed using a Frontier FT-IR Spectrometer made by Perkin Elmer with the Universal ATR sampling accessory. Its spectral region ranges from $250cm^{-1}$ to $8300cm^{-1}$. The spectral analysis was restricted from $400cm^{-1}$ to $4000cm^{-1}$ since the vibrational frequencies of the molecular bonds present in the analyzed solution encompassed those boundaries [75]. The calibration for this device was done using a background scan. Each measurement was performed by pipetting 3µl of the sample directly on the ATR crystal. This process was repeated 4 times. Measures for both techniques were performed at RT.

5.3 – Sensor and Optical Fiber Assembly and Measurement

The commercial sensors used in this study are very simple units that lack any sampling system or structural support. Both these features were needed to convey measurements and so, a custom-made sampling and support system was developed. The sampling entailed pipetting 4.3ml of the desired solution into a glass full clear face spectrophotometric cuvette from Starna Cells that was placed in a supporting structure. The dimensions of the cuvette were: 13

mm x 13 mm x 47 mm. The chosen volume guarantees the maintenance of an optimal focal distance for the sensors.

Due to the optical nature of the sensors, external light stimuli can be highly disruptive for the measurements. Thus, a confinement system was developed to restrict the received electromagnetic radiation to the sensors own emitters. This system consisted on the design of an assemblable supporting structure for both the cuvettes and the sensors and later 3D printed in a black PLA polymer. A black pigment has the highest absorption ratio which guarantees that all the received reflected radiation comes from the measurand and therefore the choice of color. This structure is divided into 3 main components: a personalized base structure where the sensor is held in place and the cuvette is inserted, a body section that confines the cuvette height in its extension and a lid which further helps to fixate the cuvette in a given position and serves as a closing mechanism (Figure 5.1 A). To enhance precision and minimize drift from cuvette placement, a universal socket with exactly 13mm of inner face size was also printed fitting in every sensor base (Figure 5.1 B). Furthermore, since every sensor has different physical dimensions and shapes, 5 custom bases were designed and printed, one for each sensor. However, all the bases shared as common coupling mechanism that allowed the usage of the same body and lid parts with every sensor, minimizing the introduction of systematical errors in the measurement. The interchangeable nature of this structure allows for easy cuvette replacement and quick sensor change.

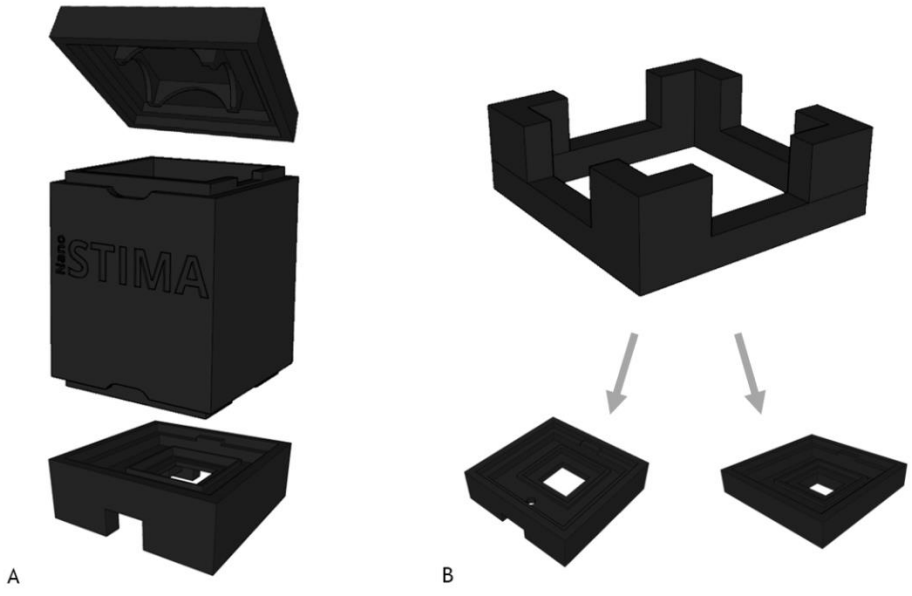

Figure 5.1 - Supporting sensor structure: A - Exploded view of the whole structure; B - Universal socket and example of matching bases

The disposition presented in Figure 5.2 (right) illustrates a setup for measuring the target solution through the cuvette's glass base. Alternatively, the presented structure can be flipped upside down for measuring the solution directly (fig 5.2, left picture). For nomenclature purposes, the conformation displayed on Figure 5.1-A will be addressed, from now on, as "regular"

and its upside-down counterpart as “inverted”. Since there is no prior evidence of any setup’s advantages over the other, both methods were equally tested.

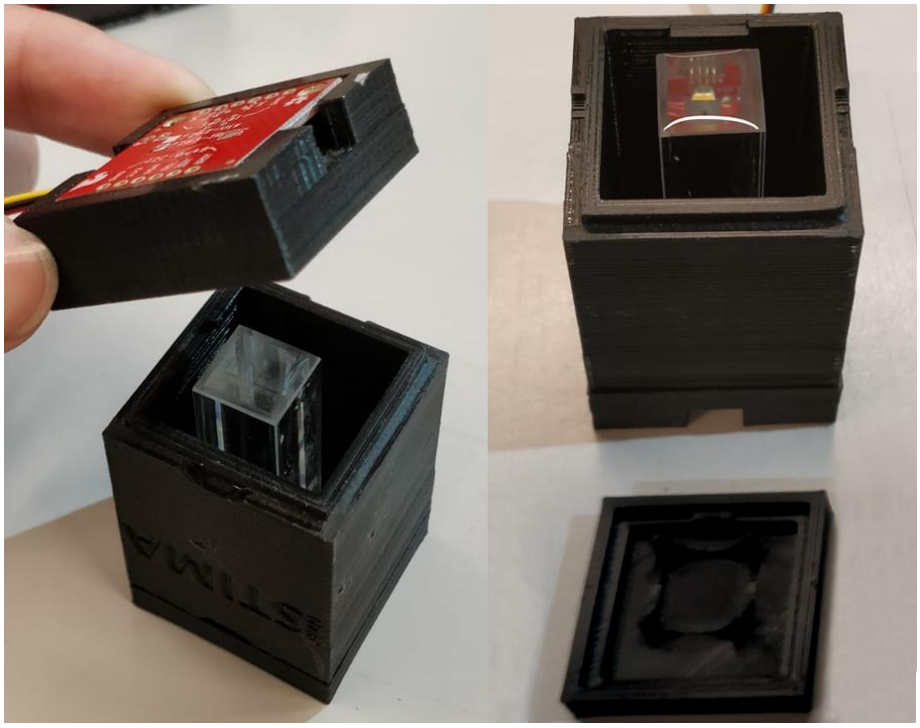

Figure 5.2 - Measuring setups for the optical sensors: Regular (right) vs inverted method (left)

All the experiments were carried out in laboratory environment at INESC-TEC at room temperature with minimal drift over time and calibration was performed for each individual sensor using deionized water. It was also established that every measurement would encompass 50 instances of the sensor’s output that would then be converted to a mean value. Unlike the other sensors, the VCNL4020 is heavily affected by noise at the beginning of the measurement, this way, a total of 300 instances per measurement were established for this sensor to allow greater stabilization. Every measurement was repeated 4 times (n=4). Furthermore, statistical analysis was thoroughly performed using One-way ANOVA with post hoc Tuckey HSD test which compared both groups of samples and groups of series to assess statistical separability. This is indicated by the asterisk (*) symbol on top of each graph. One asterisk (*) implies $p<0.05$, two asterisks (**) implies $p<0.01$ and three asterisks (***) implies $p<0.001$. As stated, all statistical analysis was conducted in the software GraphPad. This process is visually displayed in fig.5.2.

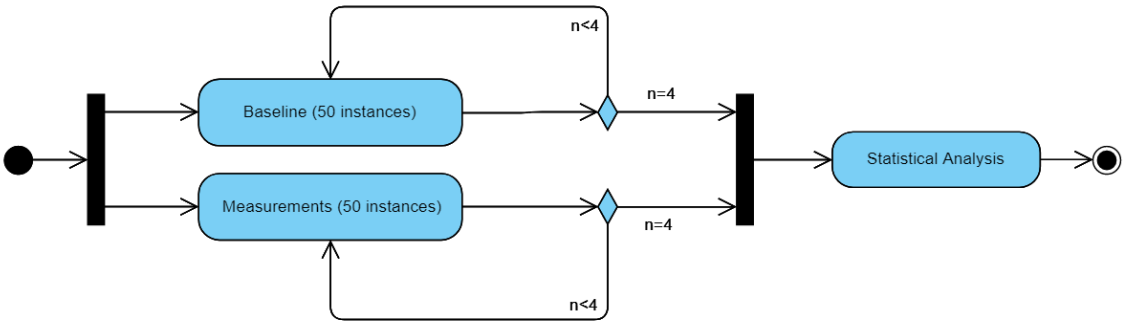

Figure 5.3 - Measurement pipeline process

For the optical fiber analysis, the optical fiber setup described in chapter 4 was used. For sampling in this system, 100µl of the desired solution were pipetted on a microscope slide that was fixed on the fiber stand. The fiber tip was then inserted on the sample and 50 instances were recorded. This process was repeated 4 times. The microscope slide was thoroughly cleaned before and in-between measurements. The calibration of this method was also performed by inserting the fiber tip into deionized water following the described method.

5.4 – Summary

In this chapter, the compound selection was addressed and quantified. The solution preparations were covered and the mixtures comprising the artificial sweat were unveiled. Both spectral methodologies were described in regard to the practical processes as well as the reasoning behind the selected tests and ranges.

Furthermore, the methodology of the commercial sensors and optical fiber were also addressed containing all the extra procedures necessary to the conduction of the planned tests such as the 3D printed structure.

Chapter 6

Results and discussion

This chapter covers the execution of the methodological procedures described in the previous chapter. Here, the recorded results are divided into two main sections: spectral results and sensor results. The results will be graphically displayed with statistical analysis performed on the software GraphPad.

6.1 – Spectral results

In this section, the results for the UV-VIS and ATR-FTIR spectral measurements will be displayed, starting with the single-compound spectrums and the finishing with the artificial sweat spectral comparisons for two relevant sweat concentrations (medium and maximum) as described in the previous chapter.

The aim of the wide-spectrum analysis was to identify and pinpoint interest zones of the electromagnetic spectrum. This way, specific wavelengths that would produce the highest amplitude signal for a certain component could be exploited by the commercial sensors. In this sense, the UV-VIS was used for the visible light and NIR spectrum, strategically avoiding the UV part of the spectrum since peaks in these wavelengths could not be safely analyzed in-vivo, and the ATR-FTIR spectroscopy was used to cover the IR part of the spectrum. It is important to note that the NaCl solution was not profiled with this technique since it would not be adequate as the NaCl particles in solution do not possess any molecular bonds [76].

6.1.1 – UV-VIS

The UV-VIS results are displayed in a 2-axis dispersion graph having the absorbance values displayed on the y-axis and the different wavelengths in the x-axis starting from 400nm up to 900nm.

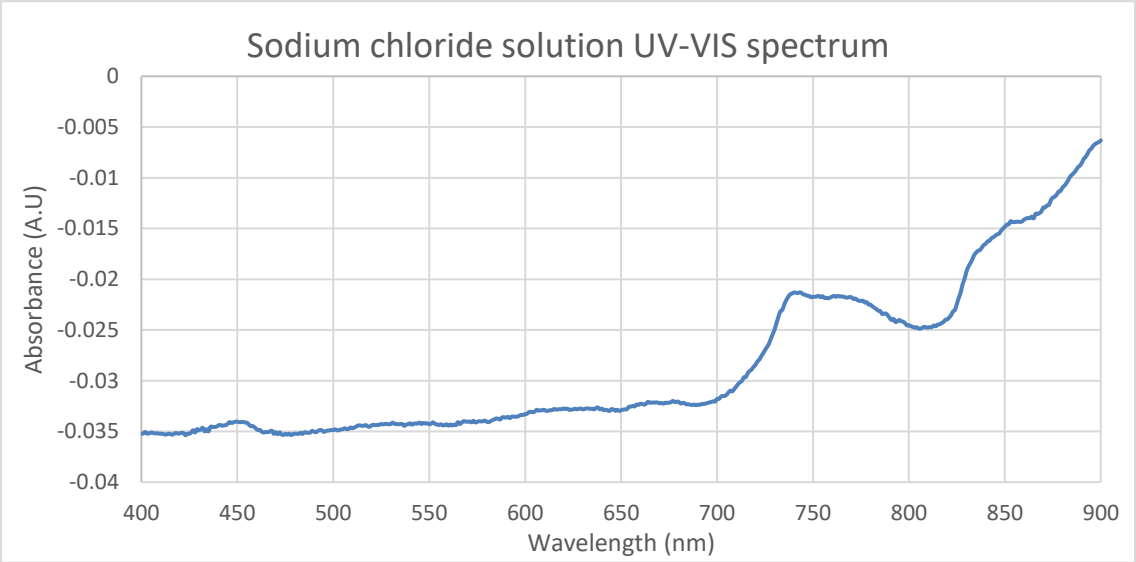

Figure 6.1 – Sodium chloride solution UV-VIS spectrum

The sodium chloride solution spectrum was entirely comprised of negative absorbance values which saw a slight increase with the increase in wavelength size being the main increase points from 700nm and 820nm. It also did not present any notable peaks as the absorbance range was very narrow only encompassing an interval of 0.0291 absorbance units.

The urea solution spectrum presented an even narrower absorbance range with maximum values of 0.0003 and minimum values of -0.0012 at 462nm and 832nm respectively. Due to the

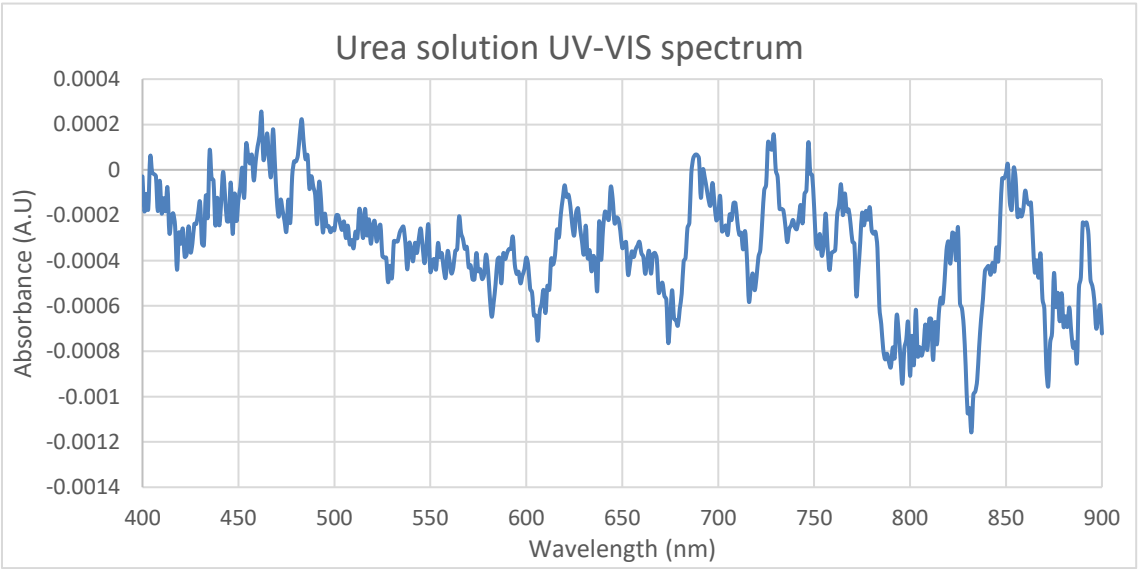

Figure 6.2 – Urea solution UV-VIS spectrum

very small absorbance values, no peaks of interest could be identified. There are also small variations of absorbance values in the lower wavelengths that get progressively more dispersed from around 670nm onwards.

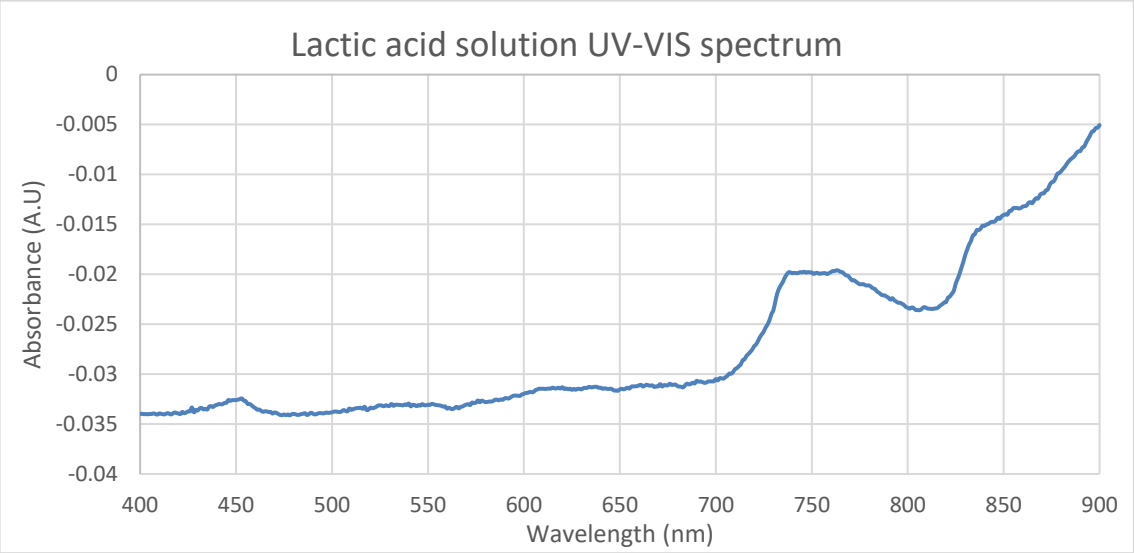

Figure 6.3 – Lactic acid solution UV-VIS spectrum

The lactic acid solution spectrum follows a very similar trend to the sodium chloride spectrum. However, these values were consistently higher in this spectrum comprising a range of absorbances from -0.0341 at 400nm to -0,0051 at 900nm. The rise of the absorbance values also matches the trend in the NaCl spectrum at 700nm and 820nm. Despite the consistently higher values of this spectrum over the NaCl, this spectrum was still encompassed in negative values contrary to the urea spectrum.

The artificial sweat solutions presented a similar trend both with very small and negative absorbance values throughout the spectrum. However, the medium concentration spectrum presented consistently higher values of absorbance than the maximum concentration spectrum. Moreover, the medium concentration spectrum presented little oscillation in its absorbance across the spectrum. Conversely, the maximum concentration artificial sweat solution presented an absorbance decaying behavior with the increase in wavelength.

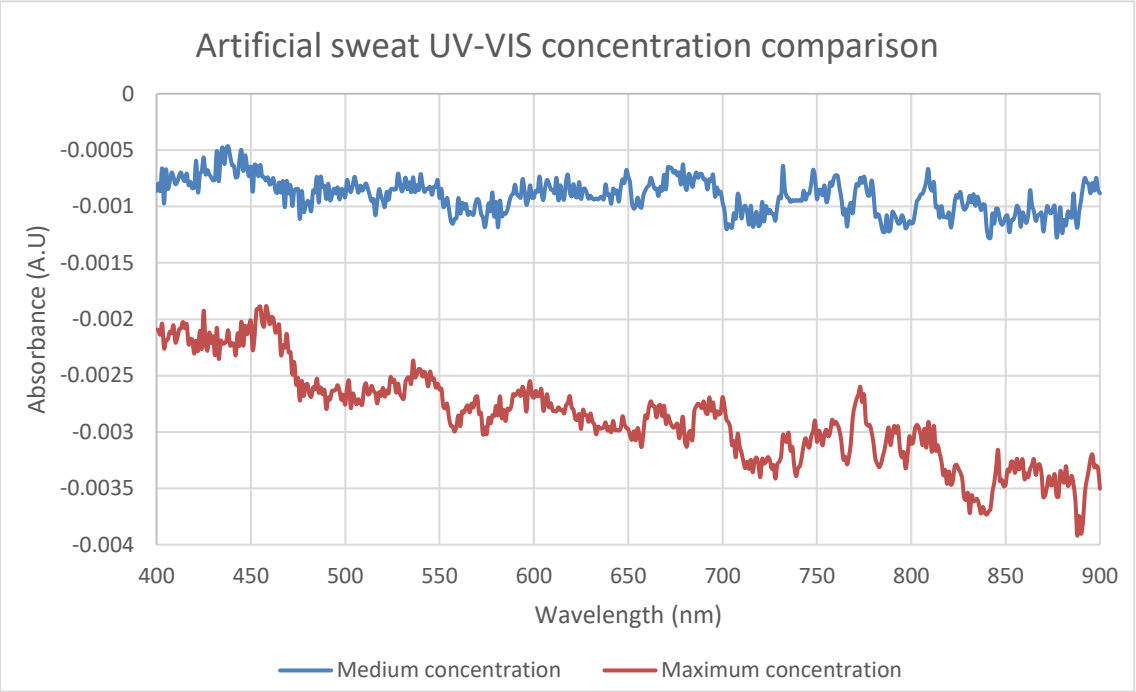

Figure 6.4 - Artificial sweat UV-VIS concentration comparison

In summary, the UV-VIS results showed spectrums with narrow absorbance ranges and very slightly negative absorbance values which have no physical meaning. These seen fluctuations were most likely due to internal machine noise. As expected, both the single-compound and the artificial sweat solutions were translucid concoctions and therefore completely invisible to the range of electromagnetic waves established on the UV-VIS spectrophotometer. These results show that absorbance spectroscopy in this determined range is not a good assessment tool for sweat monitoring.

6.1.2 - ATR-FTIR

The ATR-FTIR results are displayed in a 2-axis dispersion graph having the transmittance percentage values displayed on the y-axis and the different wavelengths in the x-axis starting from 400cm^{-1} to 4000cm^{-1} which is the typical unit of infrared spectroscopy which corresponds to a range from 25000nm to 2500nm.

The urea infrared spectrum (displayed in fig.6.5) presented significant well-defined peaks in various wavelengths. From right to left, transmittance starts at nearly 100% but suffers a big depression at 3700cm^{-1} peaking at 3306cm^{-1} with a transmittance percentage of only 49%. From this point it quickly ascends back to the former value. The second major peak comes at 1631cm^{-1} with 66% transmittance. From here, two smaller, yet notable peaks are shown at 1468cm^{-1} and 586cm^{-1} with transmittance percentages of 92% and 89% respectively.

The lactic acid infrared spectrum (also presented in fig.6.5) shared many similarities with the urea spectrum but also presented unique differences to the previous spectrum. From right to left, transmittance starts again at 100% but also suffers a big depression peaking at 3306cm^{-1} with a transmittance percentage of 51% and, similarly, ascends back to the former value. The second major peak comes at 1636cm^{-1} with 74% transmittance, however, the depression leading to this peak suffers a slight inflexion between 1660cm^{-1} and 1670cm^{-1}. The most notable differences between the two spectrums reside in the notable reduction of the aforementioned 1468cm^{-1} peak and the appearance of a notable peak at 1132cm^{-1} comprising 93% transmittance. Finally, the last notable peak is shown at 595cm^{-1} with a transmittance of 87%.

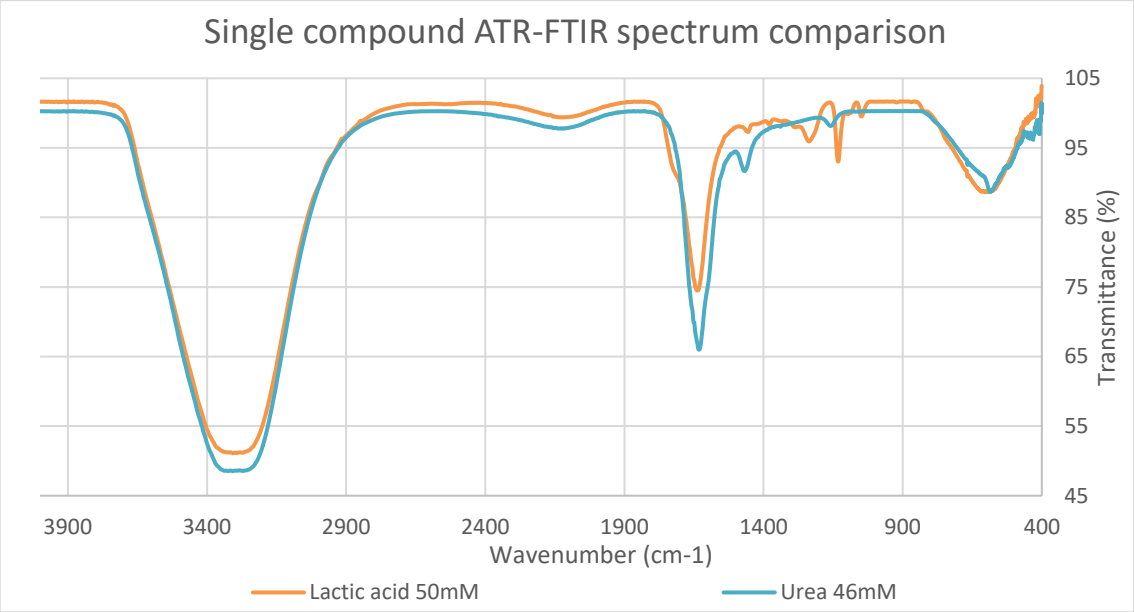

Figure 6.5 - ATR-FTIR lactic acid and urea spectrum comparison

The results from both the urea and the lactic acid solutions showed promising spectrums regarding their compositional nature. Both solutions presented a common peak at around 1631cm^{-1} which is most likely referred to the double covalent bond stretching between Carbon and Oxygen (C=O) which is present in both compounds [75]. Since it is a peak shared by more than one compound, it is not a good standalone biomarker indicator. However, given that it is present in both sweat compounds, the same molecular bond count is increased which may help discriminate human sweat from other substances in small sweat concentrations.

The obtained spectrums also presented unique peaks for both the urea and the lactic acid solutions. The exclusive urea peak registered at 1468cm^{-1} is most likely caused by the single covalent bond bend between carbon and nitrogen (C-H) while the exclusive lactic acid peak registered at 1132cm^{-1} is most likely triggered by the stretching of the single covalent bond between carbon and oxygen (C-O). Contrary to the common peak, these exclusive peaks can potentially serve as dedicated study regions for the compositional discrimination of urea and lactic acid in biofluids.

On the other hand, the different concentrations of the artificial sweat solutions showed little differences having their spectrums almost completely overlapped except for the peak presented at 595cm^{-1} which presented lower transmittance values for the medium concentration solution (88%) and higher values for the maximum concentration sweat solution (90%).

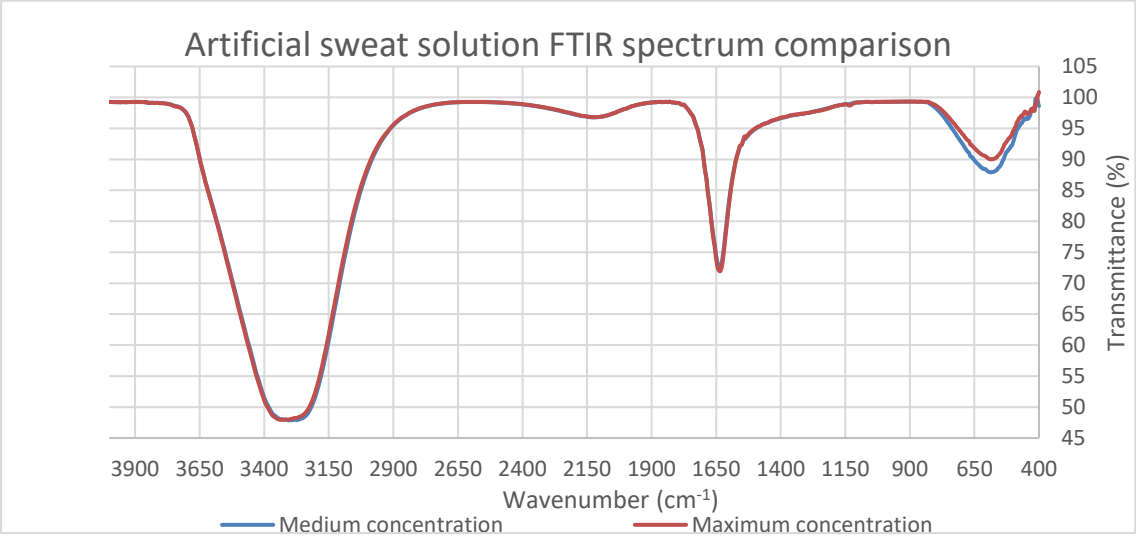

Figure 6.6 - Artificial sweat solution FTIR spectrum comparison

The differences registered in the 595cm^{-1} peak were unique to the artificial sweat solutions and were not registered in the Urea and Lactic acid spectrums. These results raised the question of what component would be causing the transmittance drift at this peak. Since, according to the literature [75], both tested components did not have any molecular bonds that vibrated at that wavelength, the remaining component, NaCl, would be the remaining candidate to explain such effect. Furthermore, studies have shown that salts such as NaCl have an active effect on the solvation of an aqueous solution [77]. Considering this, new ATR-FTIR spectrums were conducted using the medium concentration of artificial sweat and varying its NaCl content until reaching the NaCl concentration present in the maximum concentration of artificial sweat. Four concentrations of NaCl were used to meet this end: 3.1*10^{-1}g/mol (medium sweat concentration), 1.24*10^{-1}g/mol, 2.68*10^{-1}g/mol and 3.9*10^{-1}g/mol (maximum sweat concentration).

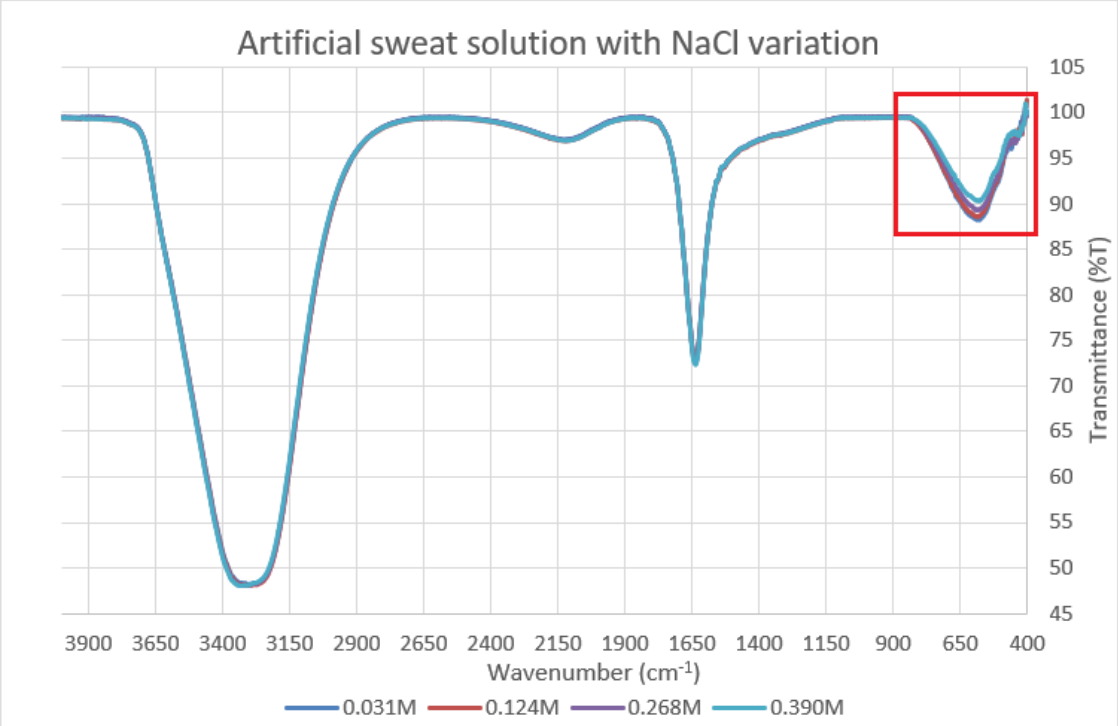

Figure 6.7 – Artificial sweat solution with NaCl variation

The resulting spectrums are displayed on fig.6.7 and a close-up of the interest peak (highlighted by the box in fig.6.8) can be inspected in fig.6.8. The close-up of the artificial sweat spectrums with NaCl variation showed a trend in transmittance with the increase of NaCl in the medium concentration artificial sweat solution. The transmittance of the artificial sweat rises with the increase of NaCl in the solution. Using the 595cm^{-1} peak information, the different concentrations of NaCl used were plotted against their respective transmittance values and a linear regression was performed. The resulting regression showed a very significant R^2 value of 0.982. These results showed that NaCl was the most likely responsible for the shift of the 595cm^{-1} peak in the artificial sweat solution FTIR spectrum and that the calibration curve designed with different NaCl concentrations can potentially be used as a salinity prediction tool for human sweat.

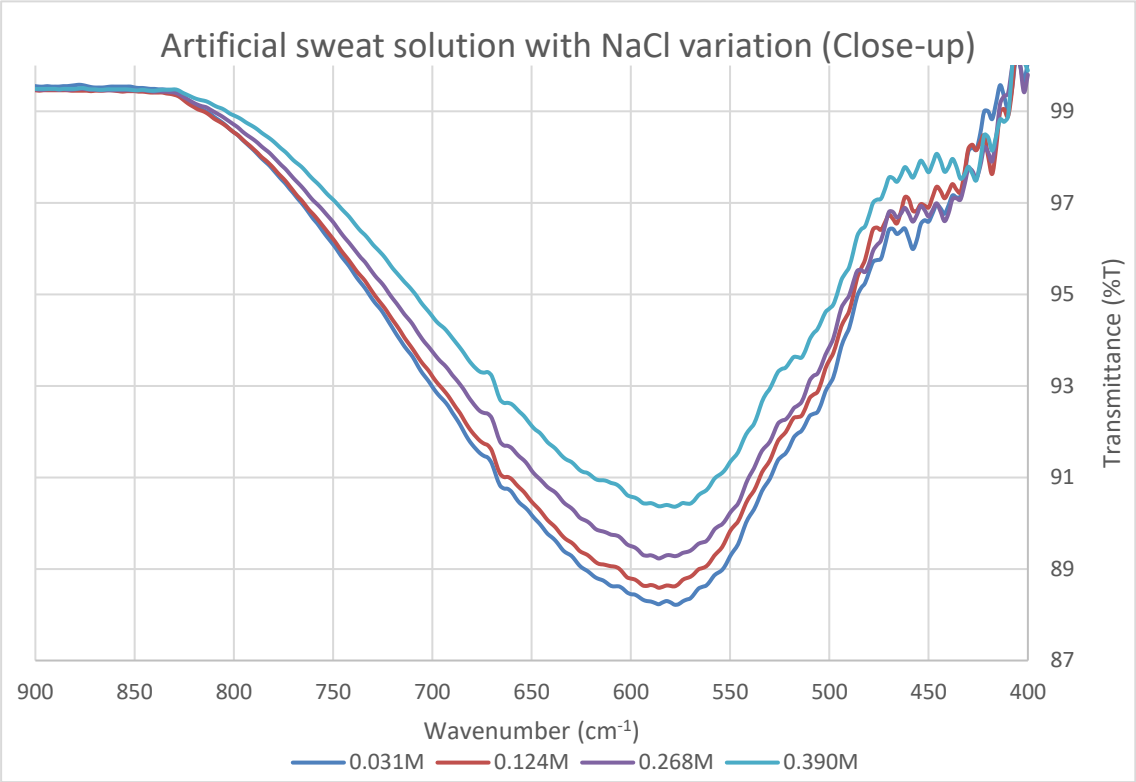

Figure 6.8 - Artificial sweat solution with NaCl variation (Close-up)

6.2 – Sensor results

The optical sensor results were organized by wavelength emission and both measuring methods (regular and inverted) were compared. The results are displayed in bar graphs with their respective error bars. The x-axis represents the measured solution and the y-axis represents the relative luminous intensity which is a function of the measured intensity divided by the intensity of the baseline (water), therefore all the "water" labeled series have an established intensity of 1 for comparison purposes. Additionally, it is important to note that the measured luminous intensity is proportional to the reflectivity of the sample (considering the sensor's functionality). Moreover, the graphical information was organized in tables which allows for easy information access. Here, each wavelength in the respective method is characterized in regard to its statistical relations and to the overall trend based on luminous intensity (in ascending order).

6.2.1 – Single compound solution

The single-compound solution measurements aimed at assessing each sensor's response to NaCl, urea and lactic acid in solution at their respective biological concentrations in human sweat. Here, the author intended to investigate whether different components would produce different responses and if these responses followed an overarching trend or relation to the baseline measurements.

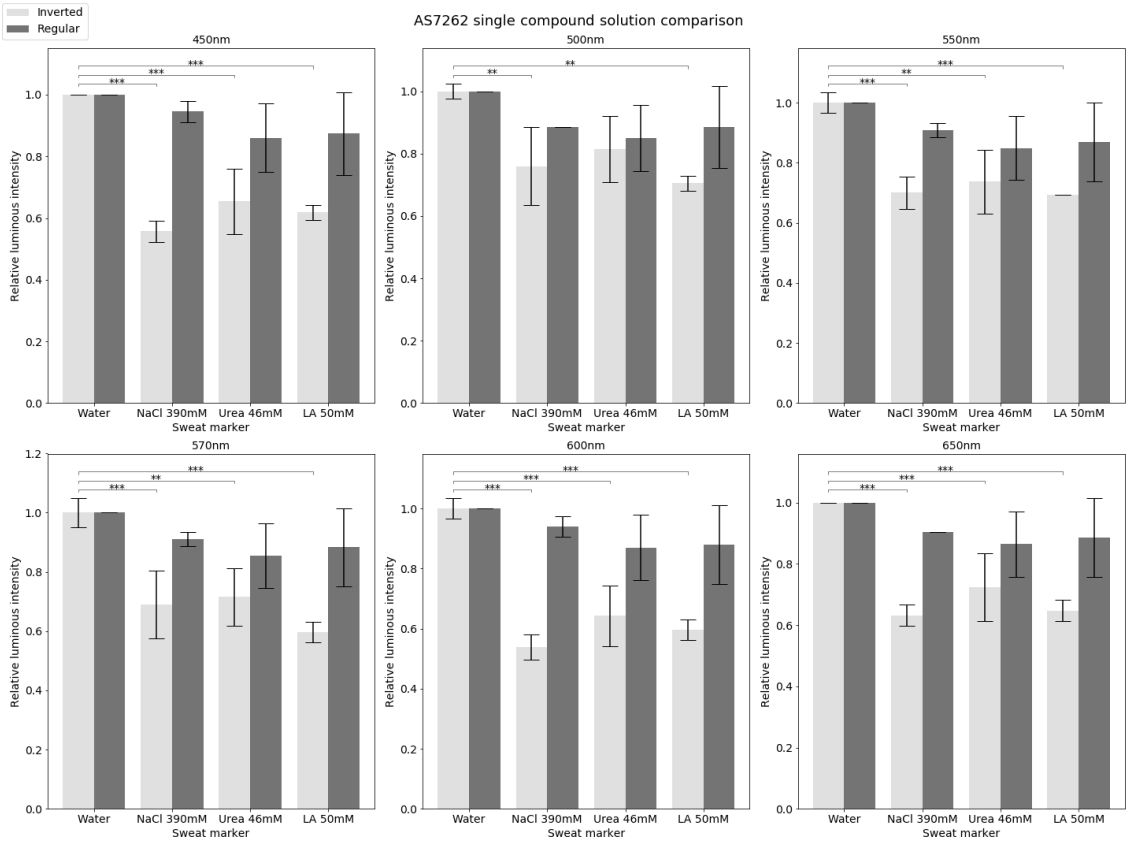

Figure 6.9 – AS7262 single compound solution comparison

The results for the single compound solution measurements of the sensor AS7262 are displayed in fig.6.9. The single compounds solutions showed lower values of luminous intensity compared to the baseline, both in the regular and the inverted method, a behavior which is verified in every wavelength for this sensor. Moreover, despite not statistically relevant, the three tested solutions followed a similar pattern over all the tested wavelengths, being the urea solution the most reflective in all the cases. A comparison between wavelength behaviors can be visualized in table 6.1. For the inverted method, the single compound solution measurements showed statistical separability between the baseline (B) and all the compounds ($p<0.01$ or lower) for all measured wavelengths except at 500nm. Here, there was only statistical separation between the baseline and NaCl and between the baseline and lactic acid.

Table 6.1 - AS7262 statistical relation table for the single compound solution measurements

Method	Wavelength	Statistical Separation	Trend
Inverted	450nm	B - All	All < B
	500nm	B - NaCl ; B - LA	NaCl < B ; LA < B
	550nm	B - All	All < B
	570nm	B - All	All < B
	600nm	B - All	All < B
	650nm	B - All	All < B
Regular	450nm	-	-
	500nm	-	-
	550nm	-	-
	570nm	-	-
	600nm	-	-
	650nm	-	-

B – Baseline; LA – lactic acid; NaCl – Sodium Chloride; All – Remaining comparisons

Overall, the regular results did not present any statistical separability. On the other hand, using the inverted method, the AS7262 was capable of discerning water from the other tested biomarkers in solution in almost every wavelength. Furthermore, all the tested solutions presented lower luminous intensity values than the baseline.

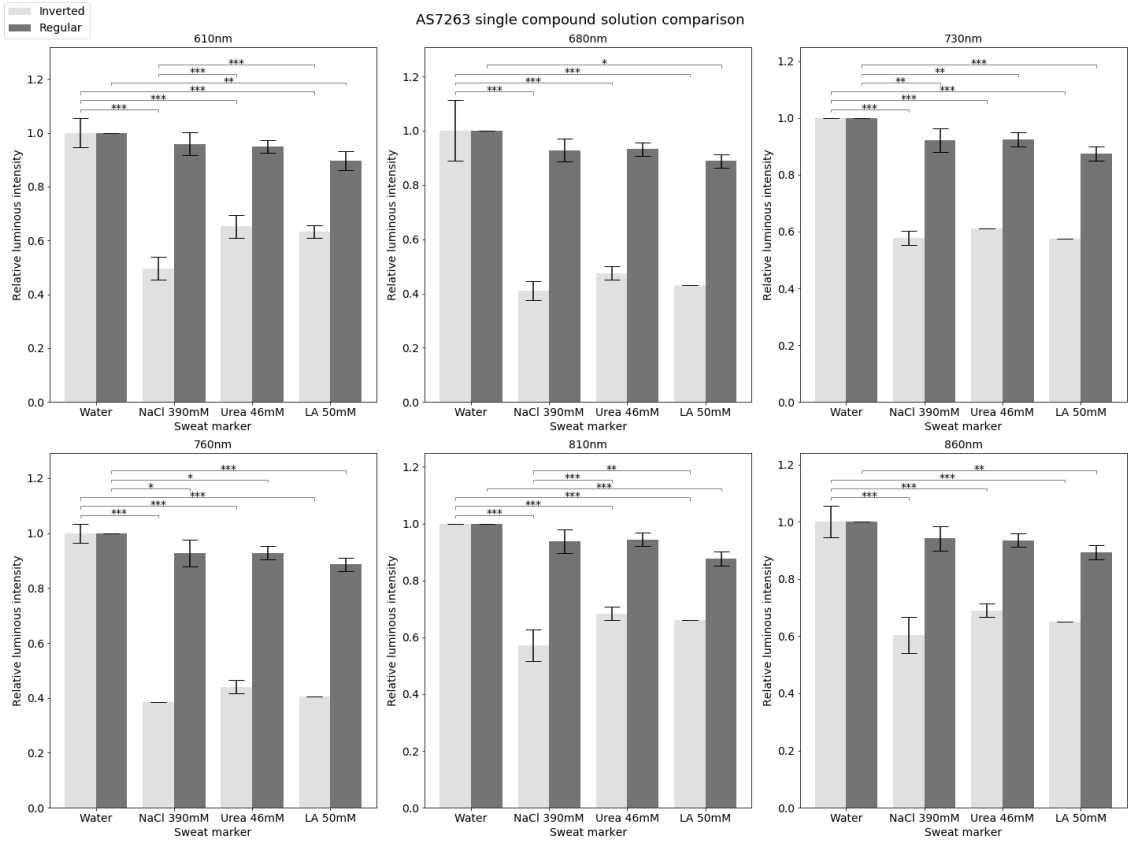

Figure 6.10 - AS7263 single compound solution comparison

The results for the single compound solution measurements of the sensor AS7263 are displayed in fig.6.10. Much like the former sensor, these measurements showed lower values of luminous intensity compared to the baseline, both in the regular and the inverted method, for all the sensor's wavelength.

Statistical relations for this sensor are displayed in table 6.2. For the inverted method, the single compound solution measurements showed statistical separability between the baseline and all the compounds ($p<0.001$). Furthermore, at 610nm and 810nm, these measurements also showed statistical separability between NaCl and both remaining sweat compounds ($p<0.01$ or lower) being that, at these wavelengths, NaCl possessed the lowest reflectance values of all the compared solutions.

Regular measurements showed reduced separability between the baseline and the single compound solutions given that most results only showed statistical separability between the baseline and the lactic acid solution ($p<0.05$ or lower). Separability between the baseline and all the compounds was only achieved at 730nm and 760nm.

Table 6.2 - AS7263 statistical relation table for the single compound solution measurements

Method	Wavelength	Statistical Separation	Trend
Inverted	610nm	B - All ; NaCl - Urea ; NaCl - LA	NaCl < Urea < B ; NaCl < LA < B
	680nm	B - All	All < B
	730nm	B - All	All < B
	760nm	B - All	All < B
	810nm	B - All ; NaCl - Urea ; NaCl - LA	NaCl < Urea < B ; NaCl < LA < B
	860nm	B - All	All < B
Regular	610nm	B - LA	LA < B
	680nm	B - LA	LA < B
	730nm	B - All	All < B
	760nm	B - All	All < B
	810nm	B - LA	LA < B
	860nm	B - LA	LA < B

In summary, using the inverted method, the AS7263, much like the AS7262, was capable of discerning water from the other tested biomarkers in solution. In fact, this NIR sensor performed better than his visible counterpart as the difference in luminous intensity between the baseline and the tested solutions was greater with this sensor. The regular results were, once again, unremarkable. This suggests that the inverted method is, once again, a better methodology alternative to use with this sensor. It is also important to notice that the statistical separability observed between the different biomarker's solutions does not necessarily mean that the sensor can discriminate one biomarker from another. In fact, given that the solutions had different concentration compositions, the difference in luminous intensity may be caused by the concentration differences of the biomarker solutions and not by the type of biomarker itself.

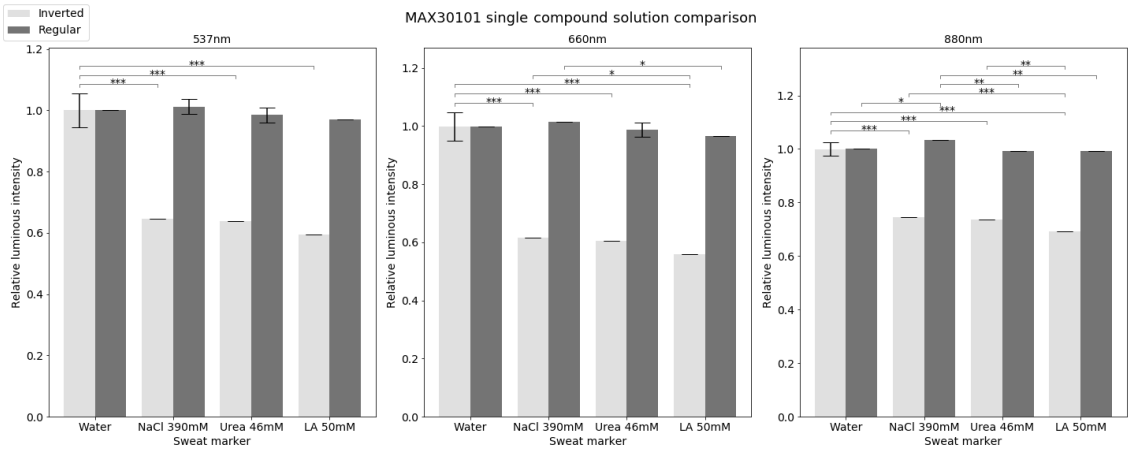

Figure 6.11 – MAX30101 single compound solution comparison

The results for the single compound solution measurements of the sensor MAX30101 are displayed in fig.6.11. The single compounds solution results showed consistent lower values of luminous intensity compared to the baseline for the inverted measurement only. Statistical relations for this sensor are displayed in table 6.3. For the inverted method, the single compound solution measurements showed, like the AS7263, statistical separability between the baseline and all the compounds ($p<0.001$). However, at higher wavelengths (660nm and 880nm) results showed statistical separation between lactic acid and NaCl while at the highest wavelength (880nm) it also showed separation between lactic acid and urea. It is also noteworthy that despite its statistical separability, the Lactic acid solution showed the lowest luminous intensity of all the samples across all wavelengths.

Regular results showed an increase in statistical separability with the increase in wavelength. Ranging from no separability (at 537nm) to statistical difference between NaCl and all the remaining solutions and baseline (at 880nm). Furthermore, using this method, the registered NaCl luminous intensity values were greater than the baseline throughout the sensor's wavelengths.

Table 6.3 - MAX30101 statistical relation table for the single compound solution measurements

Method	Wavelength	Statistical Separation	Trend
Inverted	537nm	B - All	All < B
	660nm	B - All ; NaCl - LA	LA < NaCl < B
	880nm	B - All ; NaCl - LA ; Urea - LA	LA < NaCl < B ; LA < Urea < B
Regular	537nm	-	-
	660nm	NaCl - LA	LA < NaCl
	880nm	NaCl - All	All < NaCl

Overall, this sensor was more efficient at distinguishing the single compound solutions using the inverted method over the regular method. It is also conspicuous that the overall performance of the MAX30101 increased at bigger wavelengths being 880nm the wavelengths that produced most separability between the baseline and the sweat biomarker's solution and between different biomarker solutions.

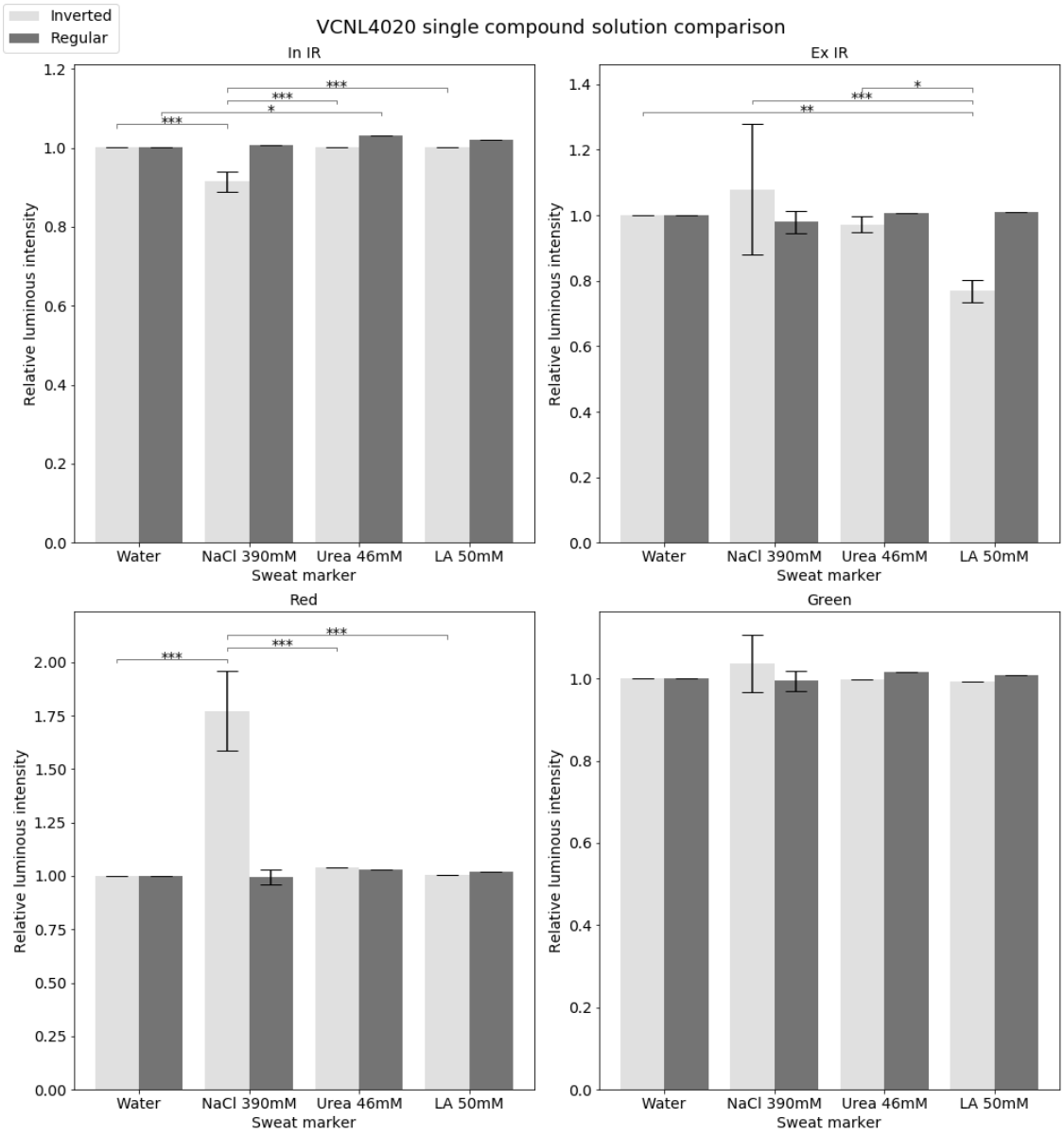

Figure 6.12 – VCNL4020 single compound solution comparison

The results for the single compound solution measurements of the sensor VCNL4020 are displayed in fig.6.12. For the inverted method, in contrast to previous results, statistical separability was not established between the baseline and the sweat compound solutions. Statistical comparison in table 6.4 showed that separability existed between one of the solutions and the remaining samples (including baseline). Instead, results showed statistical separation between NaCl and the remaining samples using the In IR and the Red emitters (890nm and 660nm respectively) and separation between lactic acid and the remaining samples using the Ex IR emitter (940nm). The green emitter (525nm) showed no statistical separation. Furthermore, the NaCl luminous intensity values showed opposing trends in their mentioned separability occurrences being more reflective than water at 660nm (Red) and less reflective at 890nm (In IR).

The regular results showed no statistical relevant relations in almost every wavelength apart from distinguishing urea from the baseline at 890nm (using the In IR emitter).

Table 6.4 – VCNL4020 statistical relation table for the single compound solution measurements

Method	Wavelength	Statistical Separation	Trend
Inverted	In IR (890nm)	NaCl - All	NaCl < All
	Ex IR (940nm)	LA - All	LA < All
	Red (660nm)	NaCl - All	All < NaCl
	Green (525nm)	-	-
Regular	In IR (890nm)	B - Urea	B < Urea
	Ex IR (940nm)	-	-
	Red (660nm)	-	-
	Green (525nm)	-	-

In summary, despite presenting several instances of statistical separability, this sensor produced inconsistent results across its operating wavelengths. Furthermore, the unexpected behavior of the VCNL4020 in the inverted measurements did not follow the trend set by the previous sensors in similar wavelengths. Finally, the regular results didn't register any significant differences between solutions and the baseline, across all the wavelengths.

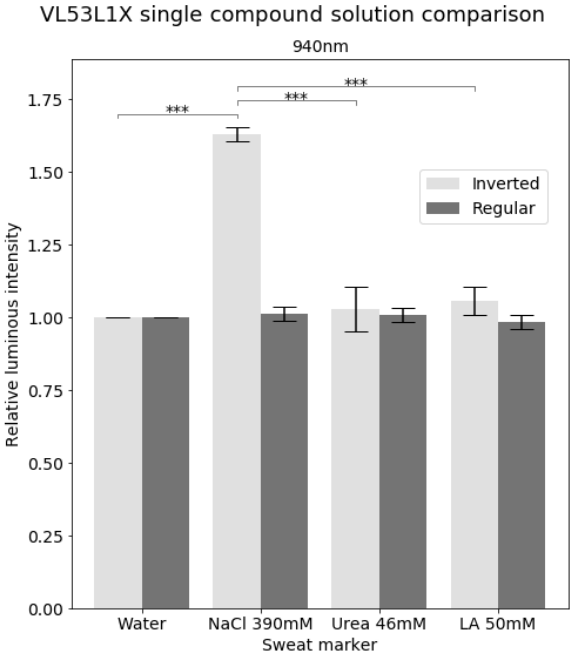

Figure 6.13 – VL53L1X single compound solution comparison

The results for the single compound solution measurements of the sensor VL53L1X are displayed in fig.6.13. At the operating wavelength (940nm), the sensor showed a very similar behavior to what was observed at 660nm in the VCNL4020 (using the red led). The luminous intensity values for all the solutions were very similar to the baseline values except for the NaCl solution using the inverted method where it showed a greater luminous intensity than the baseline and the remaining solutions. This behavior was traduced into statistical separability (displayed in table 6.5) between the NaCl solution and the baseline and the remaining solutions

(urea and lactic acid) with a high degree of certainty ($p<0.001$). The regular results showed no statistical separability between the samples or the baseline.

Table 6.5 - VL53L1X statistical relation table for the single compound solution measurements

Method	Wavelength	Statistical Separation	Trend
Inverted	940nm	NaCl - All	All < NaCl
Regular	940nm	-	-

The results of the VL53L1X were mostly unremarkable aside from the sensor response to the NaCl solution which attained higher luminous intensity values than the baseline. However, much like the VCNL4020, this behavior is unexpected. Since there are no additional comparable wavelengths, no further conclusions can be drawn.

6.2.2 – Artificial sweat solution

The artificial sweat solution measurements aimed at assessing the commercial sensor's response to different biologically relevant artificial sweat concentrations. With these measurements, the author intended to investigate if the mixture of the addressed components would alter the previously established response and whether the variation of solution concentration could impact sensor behavior significantly.

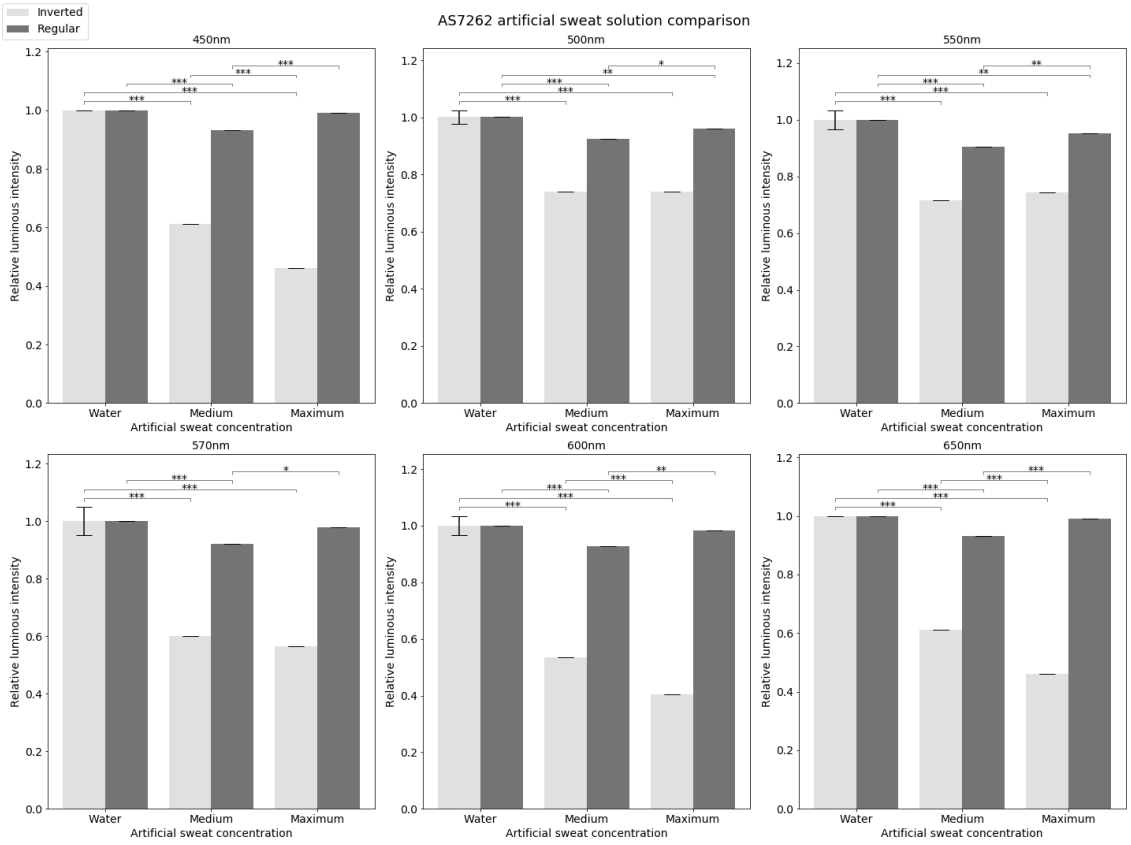

Figure 6.14 - AS7262 artificial sweat solution comparison

The results for the artificial sweat solution measurements of the sensor AS7262 are displayed in fig.6.14. For this sensor, both tested concentrations presented systematically lower luminous intensity values than the baseline for all the wavelengths. Furthermore, the maximum sweat concentration solution registered consistently lower values than the medium sweat solution using the inverted method at most wavelengths. Using the regular method, the medium sweat concentration solution registered lower luminous intensity values than both the maximum sweat solution and the baseline.

Statistical comparison in table 6.6 showed, using the inverted method, separability between the baseline and all the tested concentrations at every wavelength ($p<0.001$). Furthermore, it presented separability between artificial sweat concentrations at 450nm and from 600nm to 650nm ($p<0.001$) being the maximum concentration the less reflective.

Using the regular method, these results showed separability between the medium artificial sweat concentration and all the tested samples (including baseline) at every wavelength except between 500nm and 550nm ($p<0.05$ or lower). In this interval, all the tested samples were statistically separable, but the medium artificial sweat concentration possessed the lower reflectance values.

Table 6.6 - AS7262 statistical relation table for the artificial sweat solution measurements

Method	Wavelength	Statistical Separation	Trend
Inverted	450nm	B - All ; Med - Max	Max < Med < B
	500nm	B - All	All < B
	550nm	B - All	All < B
	570nm	B - All	All < B
	600nm	B - All ; Med - Max	Max < Med < B
	650nm	B - All ; Med - Max	Max < Med < B
Regular	450nm	Med - All	Med < All
	500nm	B - All ; Med - Max	Med < Max < B
	550nm	B - All ; Med - Max	Med < Max < B
	570nm	Med - All	Med < All
	600nm	Med - All	Med < All
	650nm	Med - All	Med < All

Max – Maximum artificial sweat concentration; Med – Medium artificial sweat concentration

Overall, the AS7262, using the inverted method, performed as expected from the previous single-compound results being able to discern water from the artificial sweat with statistical relevance. Furthermore, at certain wavelengths (450nm, 600nm and 650nm) the sensor showed statistical separability between the two tested artificial sweat concentrations. Since the compared solutions possessed the same qualitative composition, the measurements variable was tied to the concentration of the artificial sweat solutions which means that statistical separability between different concentrations of the same composition suggest that the sensor is capable of not only discerning artificial sweat from water but also to discern different concentrations of artificial sweat. Altogether, the AS7262 is a promising candidate for sweat monitoring using the inverted method.

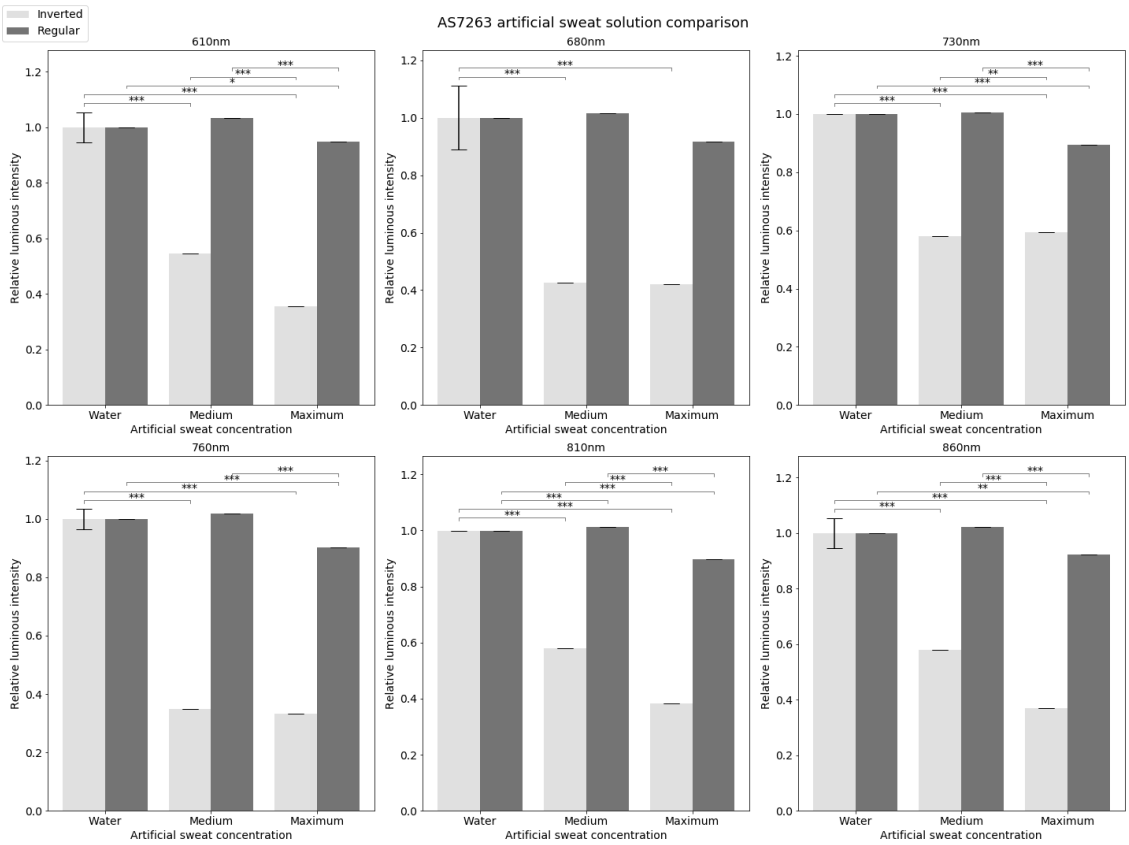

Figure 6.15 - AS7263 artificial sweat solution comparison

The results for the artificial sweat solution measurements of the sensor AS7263 are displayed in fig.6.15 and its correspondent statistical comparison in table 6.7. At 610nm, 810nm and 860nm, the inverted measurements showed a similar trend in light intensity being the baseline the highest followed by the medium concentration solution and finally the maximum concentration solution possessing the lowest luminous intensity values which were statistically relevant ($p<0.001$). Furthermore, the biggest luminous intensity differences between artificial sweat concentrations were found at 610nm and from 810nm onwards.

Additionally, the regular measurements followed a similar trend to the one verified in the AS7262. In this case, the medium concentration values were bigger than the baseline and the maximum concentration values at all the measured wavelengths. These results are incoherent with the previously displayed behaviors and as such, compromise the legitimacy of the regular method.

Table 6.7 - AS7263 statistical relation table for the artificial sweat solution measurements

Method	Wavelength	Statistical Separation	Trend
Inverted	610nm	B - All ; Med - Max	Max < Med < B
	680nm	B - All	All < B
	730nm	B - All ; Med - Max	Med < Max < B
	760nm	B - All	All < B
	810nm	B - All ; Med - Max	Max < Med < B
	860nm	B - All ; Med - Max	Max < Med < B
Regular	610nm	Max - All	Max < All
	680nm	-	-
	730nm	Max - All	Max < All
	760nm	Max - All	Max < All
	810nm	Med - All ; B - Max	Max < B < Med
	860nm	Max - All	Max < All

In summary, the AS7263 performed very similarly to AS7262 using the inverted method, presenting the same discernible capability between water and artificial sweat and being able to discern between different sweat concentrations with statistical relevance at 610nm, 810nm and 860nm. The AS7263 is another suitable candidate for sweat monitoring using the inverted method.

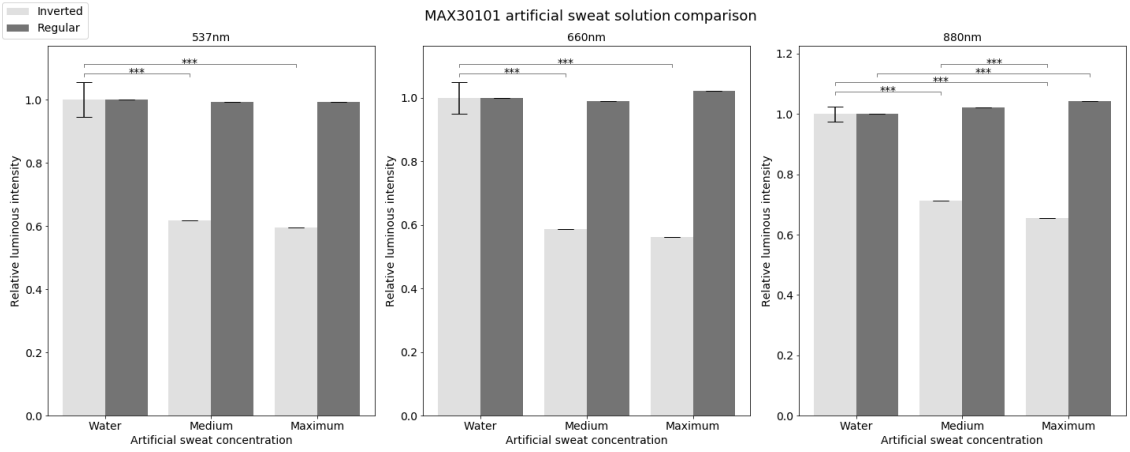

Figure 6.16 – MAX30101 artificial sweat solution comparison

The results for the artificial sweat solution measurements of the sensor MAX30101 are displayed in fig.6.16 and its respective statistical comparison in table 6.8. For all the wavelengths of this sensor, the regular method showed no statistical separability except at 880nm between the maximum concentration solution and the baseline ($p<0.001$) where the maximum concentration registered higher values of intensity than the baseline. For all the wavelengths of the inverted method, both sweat solutions showed significantly lower intensity values than the baseline being the medium sweat concentration more reflective than the maximum sweat concentration. Moreover, at 880nm, there was statistical separability between the medium and the maximum concentration solutions ($p<0.001$).

Table 6.8 - MAX30101 statistical relation table for the artificial sweat solution measurements

Method	Wavelength	Statistical Separation	Trend
Inverted	537nm	B - All	All < B
	660nm	B - All	All < B
	880nm	B - All ; Med - Max	Max < Med < B
Regular	537nm	-	-
	660nm	-	-
	880nm	Max - B	B < Max

In summary, the MAX30101 behaved similarly to AS7262 and AS7263, however, for this sensor, the statistical separability between the different artificial sweat concentrations was only statistically relevant for the largest wavelength: 880nm. The regular measurements proved unremarkable as in the previous sensors. However, for the inverted method, this sensor is a promising choice especially for usage at higher wavelengths.

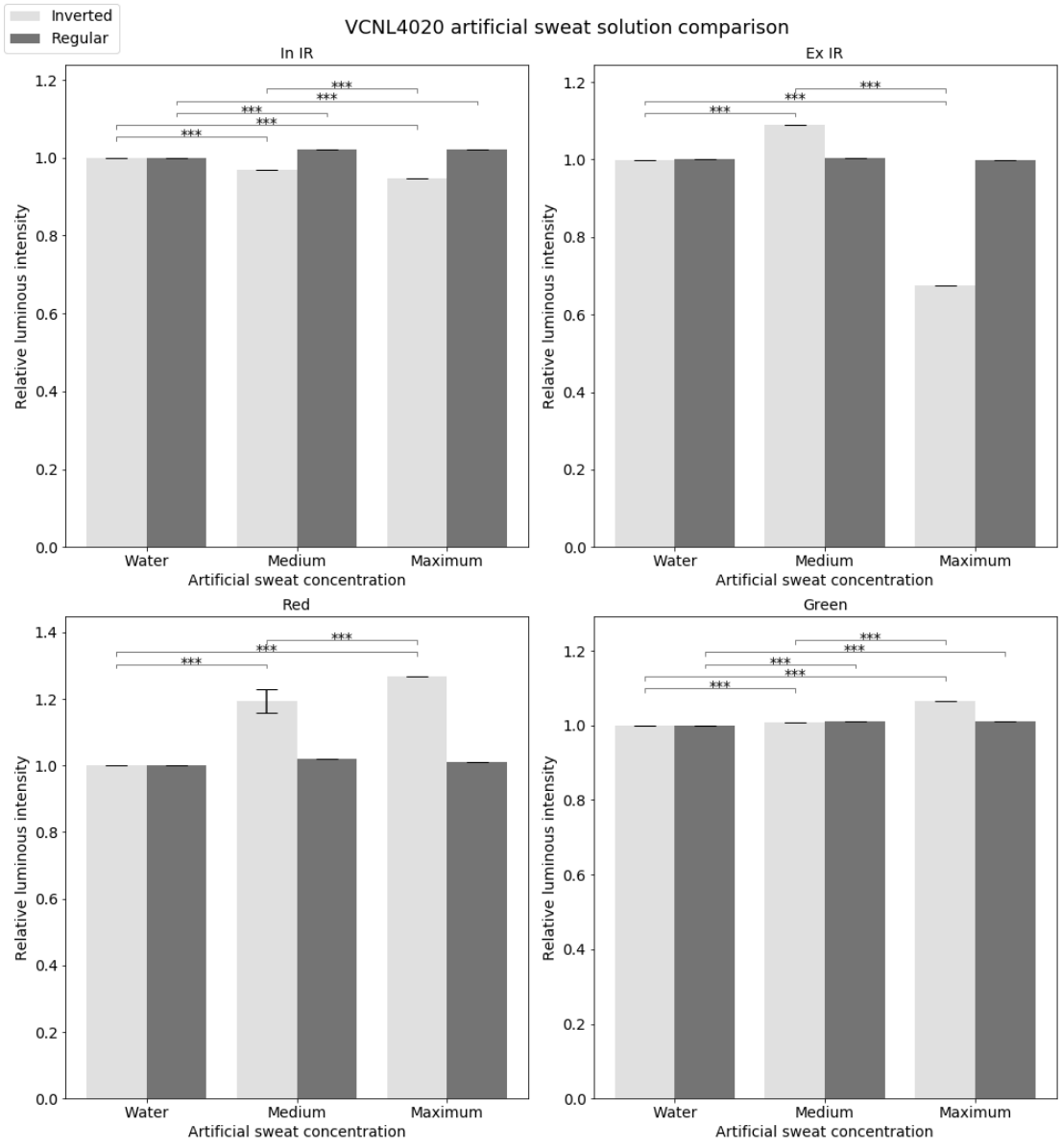

Figure 6.17 – VCNL4020 artificial sweat solution comparison

The results for the artificial sweat solution measurements of the sensor VCNL4020 are displayed in fig.6.17 and its respective statistical comparison in table 6.9. The infrared light measurements (In IR led 890nm and Ex IR 940nm) using the inverted method showed smaller luminous intensity values than the baseline except for the Ex IR medium concentration solution which was greater than the baseline with statistical significance ($p<0.001$). Both red and green LEDs (660nm and 525nm respectively) registered higher luminous intensity values for the sweat solutions than the baseline ($p<0.001$) or very similar, non-significant differences.

The regular measurements, on the other hand, did not show any noteworthy variations between the sweat solutions and the baseline with the exception of the 890nm (In IR) wavelength where it showed statistical separation between the baseline and the solutions.

Table 6.9 - VCNL4020 statistical relation table for the artificial sweat solution measurements

Method	Wavelength	Statistical Separation	Trend
Inverted	In IR (890nm)	B - All ; Med - Max	Max < Med < B
	Ex IR (940nm)	B - All ; Med - Max	Max < B < Med
	Red (660nm)	B - All ; Med - Max	B < Med < Max
	Green (525nm)	B - All ; Med - Max	B < Med < Max
Regular	In IR (890nm)	B - All	B < All
	Ex IR (940nm)	-	-
	Red (660nm)	-	-
	Green (525nm)	B - All	B < All

On the whole, the VCNL4020 did not show any improvements from the single compound measurement as it still presents inconsistent measurements using the inverted method and insignificant readings through the regular method. The statistical separations shown do not align with a specific trend which further suggests that this sensor is not suitable for sweat monitoring.

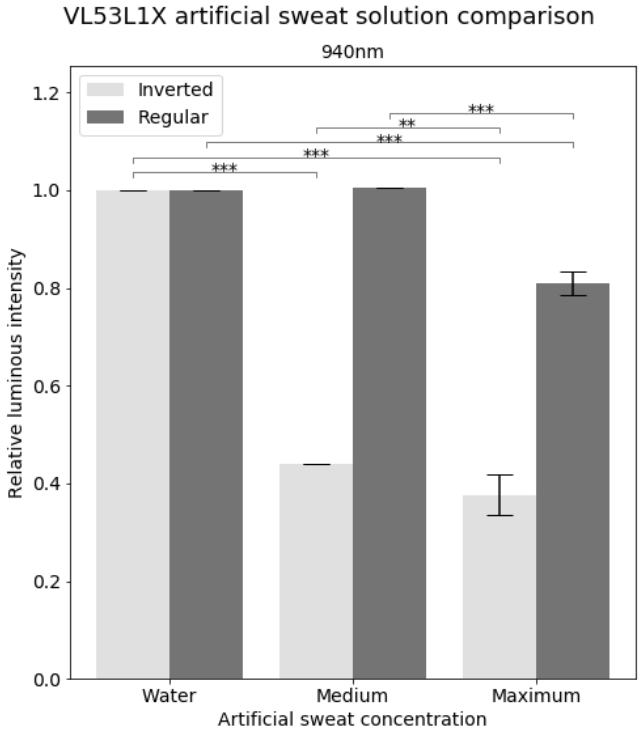

Figure 6.18 - VL53L1X artificial sweat solution comparison

The results for the artificial sweat solution measurements of the sensor VL53L1X are displayed in fig.6.18 and its respective statistical comparison in table 6.10. For the regular method, the 940nm laser showed similar luminous intensities for the baseline and the medium concentration. However, the maximum concentration intensity values were significantly lower than the other two mentioned resulting in statistical separability between the maximum concentration and both the baseline and the medium concentration values ($p<0.001$).

The inverted method showed bigger statistical separability than the former method where both the medium and maximum concentration were well below the baseline values ($p<0.001$). Furthermore, the medium concentration solution was also statistically separable from the maximum concentration solution ($p<0.01$).

Table 6.10 - VL53L1X statistical relation table for the artificial sweat solution measurements

Method	Wavelength	Statistical Separation	Trend
Inverted	940nm	B - All ; Med - Max	Max < Med < B
Regular	940nm	Max - All	Max < All

Finally, the VL53L1X showed both statistical separation between the baseline and the artificial sweat and between different artificial sweat concentrations. However, this concentration comparison was more differentiated in other sensors having a smaller, but still valid degree of certainty in this sensor ($p<0.01$) when compared to sensors like the AS7262 and the AS7263. Furthermore, the previous trends and expected behaviors established by the majority of sensors were verified in the VL53L1X. These results would suggest that this sensor would be a viable sweat monitoring tool, however, the controversial results from the single compound measurements render the usability of this sensor uncertain with further tests needed to assess the sensor true potential.

6.3 – Optical fiber

The optical fiber results for the artificial sweat solution measurements are displayed in fig.6.19. In the single compound measurements, both the urea and lactic acid solutions registered lower luminous intensity values than the baseline however only the lactic acid presented statistical separability ($p<0.01$). The NaCl solution presented higher luminous intensity values than the baseline with higher statistical relevance ($p<0.001$). The artificial sweat solutions despite registering higher luminous intensity values than the baseline that increased with the artificial sweat solution concentration, they did not carry any statistical separability.

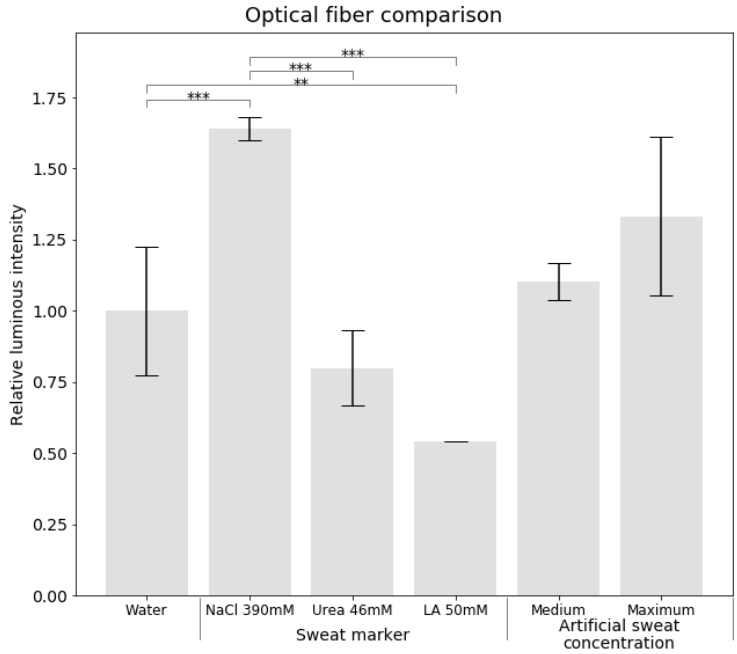

Figure 6.19 - Optical fiber comparison

Overall, there was statistical separability in the single compound solutions between the baseline and both the NaCl solution and the lactic acid solution. However, the statistical relevance of these measurements was lost in the artificial sweat solution comparison as there was no statistical separation between the baseline and the artificial sweat solutions nor between each artificial sweat concentration. These findings suggest that the used optical fiber setup does not have the necessary sensitivity to convey these measurements.

6.4 – Discussion

In this section, the obtained results will be thoroughly scrutinized in regard to the techniques and sensors used, their respective theoretical principles and the relation between these and the presented results. Furthermore, a summarized analysis of the following discussion is presented in table 6.11.

The aim of the wide range spectroscopy study was to uncover potential interest peaks across the electromagnetic spectrum for sweat analysis which could, in later studies, lead to the usage of specialized sensors at these wavelengths for sweat monitoring with wearable devices.

The spectroscopy results showed a very distinct behavior between the visible and the IR parts of the electromagnetic spectrum. The UV-VIS results covered the tested solution's response in the visible spectrum and showed that there were no significant absorbance peaks from 400nm to 900nm for all the tested single compound solutions and for both concentrations of the tested artificial sweat solutions. The displayed spectrums were even comprised mostly of negative absorbance values which carry no theoretical significance. Even if the negative results could be explained by an offset phenomenon, the very small variances across the scanned wavelengths ($A<0.0291$) further indicate that the obtained spectrums originated from

the UV-VIS equipment innate noise. These results suggest that absorbance spectroscopy in the visible spectrum is not a good strategy to develop a sweat monitoring system.

The ATR-FTIR results showed spectral differences between the two tested single-compound solutions (urea and lactic acid) while presenting overlapping regions in both spectrums. Both solutions share a peak at 1631cm^{-1} representing the C=O bond [75], which is present in both urea's and lactic acid's chemical conformation. Given this, the 1631cm^{-1} peak (equivalent to 6131nm) presents a potential sweat identification region that can be assessed by IR sensors in this wavelength. Conversely, the unique spectral urea and lactic acid peaks (1468cm^{-1} and 1132cm^{-1} respectively) represent two unique chemical bonds to these substances (C-H in urea and C-O in lactic acid [75]). These findings suggest that the usage of IR sensors that encompass the mentioned regions can potentially be used to detect urea in solution specifically at 1468cm^{-1} (equivalent to 6812nm) and lactic acid in solution at 1132cm^{-1} (equivalent to 8834nm). On the other hand, the artificial sweat solutions did not substantially retain the peaks described by the urea and the lactic acid spectrums. However, the different artificial sweat concentrations highlighted the previously overlooked 595cm^{-1} peak (equivalent to 16807nm). NaCl manipulation within the artificial sweat solution showed that this compound was the most likely responsible for the shift in transmittance at this wavelength. Furthermore, the transmittance differences registered in fig.6.8 suggest that an IR sensor within this range of wavelengths would be potentially useful in determining human sweat's salinity which could be adapted to monitor dehydration.

Regarding the commercial sensors, the goals set in this study encompassed the assessment and comparison of these sensors as potential sweat monitoring tools.

The single compound results showed consistently lower reflectance values in all tested solutions in relation to the baseline. The reflectance principles documented by Roger Clark [57], mentioned in chapter 4, state that the reflectance of a given substance is dependent on the grain size of said substance being that, the smaller particles are more reflective than larger ones. Studies on the particle size of the tested compounds (NaCl, urea and lactic acid) [78]–[80] showed that the molecular size of these compounds is significantly larger than water molecules [81]. Since the baseline is made exclusively of H_2O molecules (deionized water), the tested single compound solutions contain significantly larger particles than the baseline. According to the referred theory, since the tested solutions possess larger particles than the baseline, they should be less reflective than the baseline. The presented results corroborate Roger's findings.

Furthermore, the artificial sweat solution results also showed overall lower reflectance values than the baseline. Not only that, but the artificial sweat solution with the highest concentration (maximum biomarker concentration in sweat) also showed lower reflectance values than the lower concentrated solution (medium biomarker concentration in sweat). The behavior demonstrated in these results also supports Roger's claim as the artificial sweat solution with lower reflectance values also possesses the highest number of larger particles (maximum biomarker concentration). Both described behaviors are consistently found in AS7262, AS7263 and MAX30101 results whilst the most relevant statistical differentiation for these sensors is located between 600-650nm and 810-860nm using the inverted method. The VCNL4020 and the VL53L1X, on the other hand, showed incoherent and inconsistent results as some of the measurements showed no sensibility to the solutions while others, despite showing differences, did not follow a specific trend nor an expected behavior. Taking everything into consideration, these results highlight the potential of the AS7262, the AS7263 and the MAX30101 as viable options for sweat

monitoring as they were successfully able to discern sweat and its components from water while simultaneously being able to discern different sweat concentrations. Moreover, these results suggest that the inverted method at the described wavelengths is capable of increasing the robustness of the developed differentiation system.

Finally, the goal set for the optical fiber study was shared with the commercial sensor study: Assessing the usability of this method as a sweat monitoring tool. The optical fiber results showed very noticeable fluctuations between single-compound solution values while simultaneously not presenting any statistical separability between the artificial sweat solutions and the baseline. Despite being visually discernable in fig.6.19, this latter comparison is then disproved and overshadowed by the massive SD values which render these results inconclusive. In this sense, it is unclear whether an optical fiber system can be a viable option for sweat monitoring or not. All that be concluded is that the current optical fiber setup used in this study does not possess the required sensibility to conduct sweat measurements.

Table 6.11 - Results summary and evaluation

System	Spectral range	Interest spectral region(s)	Evaluation
UV-VIS	Vis-IR (400-900nm)	-	No potential predictive regions
FTIR	IR (2500-25000nm)	6131nm for sweat identification 6812nm for urea 8834nm for lactic acid 16807nm for sweat salinity	Potential predictive regions
AS7262	Vis (450-650nm)	450nm; 570-650nm	Suitable using the inverted method
AS7263	Vis-IR (610-860nm)	610nm; 810-860nm	Suitable using the inverted method
MAX30101	Vis-IR (537-880nm)	880nm	Suitable using the inverted method
VCNL4020	Vis-IR (525-940nm)	-	Not suitable for sweat monitoring
VL53L1X	IR (940nm)	-	Inconclusive
Optic Fiber	IR (940nm)	-	Inconclusive

Chapter 7

Conclusion and future work

In the final chapter of this thesis, a summarized report of all the topics addressed in this work will be conducted, including some additional insight regarding the motivation, objectives and results developed over the course of this. Furthermore, the future of this study will be discussed, and several paths will be explored in a section entitled “Future work”.

7.1 – Conclusion

Sweating is a mammal exclusive physiological behavior whose main function is to allow thermal regulation of an animal’s body temperature when faced with abnormally higher environmental temperatures. This process is facilitated by the eccrine and apocrine sweat glands which are tubular epithelial structures found on the skin’s inner layers. The process itself consists on the secretion of sweat by these glands following its excretion to the skin’s surface by the tubular structures of these glands. Sweat is a complex concoction of organic and inorganic components in an aqueous solution that is unique to mammals including humans.

Despite its secretion being attributed to thermo-regulatory processes, nowadays, there is a deeper interest in sweat as a potential biological marker. This is due to the fact that sweat’s components encompass a wide range of medically relevant biomarkers such as urea. Recent studies have shown that some of the biomarkers found in sweat have intricate correlations to specific physical conditions and pathologies. This way, newly non-invasive methods for monitorization and diagnosis of certain conditions using key biomarkers sampled from sweat are on the rise. Despite showing promising results, these relied heavily on colorimetrical and electrochemical approaches, which have several limitations regarding reusability and maintenance. However, these studies rely on the usage of actual human sweat which is both unpractical for testing and prone to contaminations. In this light, this dissertation aimed to both develop a method that does not rely on these principles and to synthesize a cost-effective artificial sweat with a high degree of likelihood that would then be used in an optical-oriented strategy to convey sweat’s analysis using commercially available sensors and optical fiber.

In this sense, this study started with the formulation of the artificial sweat solution based on Harvey and Stefaniak's sweat analysis from which the three of the highest concentrated components were selected: NaCl, Urea and Lactic acid. This selection was also based on the physiological importance of each biomarker, having each of the selected components a unique physiological relation (NaCl is a dehydration biomarker, Lactic acid is a muscular fatigue biomarker and urea is a pathological biomarker). Then, a selection of low-cost optical sensors and optical fiber was used to assess the potential of these methods to sweat monitoring. The experimental procedure was divided into 2 main phases: Testing the sensor's sensibility to these individual sweat biomarkers and to the developed artificial sweat solution which consisted in the mixture of the selected biomarkers in biologically relevant concentrations.

Simultaneously, two wide-range spectroscopy techniques (UV-VIS and ATR-FTIR) were used to profile the developed artificial sweat solution and to establish possible comparisons with the commercial sensors and optical fiber.

The UV-VIS results were expectedly unremarkable as the tested solutions were translucent to visible light. As such, no relevant absorbance peaks were discriminated, and it was concluded that absorbance spectroscopy in the visible spectrum was not a viable option.
The ATR-FTIR technique produced very interesting results as both organic biomarkers were profiled in the IR region which revealed interest transmittance peaks for both urea and lactic acid at 1468cm^{-1} (equivalent to 6812nm) and 1132cm^{-1} (equivalent to 8834nm) respectively. The non-overlapping peak location of these compounds suggests that the usage of IR sensors in this wavelength range could be useful for detecting these biomarkers in solution. Furthermore, the artificial sweat spectrum analysis suggested the existence of an active effect of NaCl in the amplitude of the 595cm^{-1} peak (equivalent to 16807nm). By manipulating the NaCl concentrations in the artificial sweat solution, this amplitude effect was confirmed being the NaCl the likelier causality. These results foreshadow the exploration of sweat sensors in the IR range as these sweat biomarkers have well-defined transmission regions in the IR spectrum.

Regarding the commercial sensors, as expected from the previous study, the inverted method showed sovereignty over the regular method by possessing an unmatched degree of sensibility when compared to the regular one. Furthermore, the AS7262, AS7263 and MAX30101 proved to be the most suitable sensors for sweat monitoring as they consistently displayed coherent and statistically significant behavior between the tested solutions. They were successfully able to discern the single compound solutions from water, to discern artificial sweat solution from water and able to discriminate different artificial sweat concentrations in the biological range. Furthermore, the AS7263 showed the best statistical separation between the maximum and medium artificial sweat concentrations at higher wavelengths (810nm and 860nm). The VL53L1X results proved to be inconclusive since the single compound measurements were incoherent but the artificial sweat measurements were consistent and followed the pattern of the remaining sensors, therefore, additional testing is needed to assess the usability of this sensor as a sweat monitoring tool. The VCNL4020 proved to be the less suitable sensor for sweat monitoring as it presented inconsistent and incoherent results across all of its wavelengths without ever establishing a trend nor providing statistical relevance to its measurements. Despite their differences, all the sensors provided stable readings throughout the thesis course without the need to replace any of its components. This further validates the advantages of this type of sensor over the electrochemical and colorimetrical techniques discussed in the literature review.

Finally, the optical fiber results suggested that the current optical fiber setup did not have the required sensitivity to be used as a sweat monitoring tool.

Overall, the main objectives of this thesis were successfully accomplished as the author was able to assess the potential of each commercial sensor and optical fiber as sweat monitoring tools with varying degrees of success. Furthermore, an extensive study regarding several optical techniques and mechanisms was developed as well as spectral analysis directed to sweat's study in a considerable range of the electromagnetic spectrum.

7.2 – Future work

The present study laid the foundation for the investigation of novel sweat monitoring techniques. As previously stated, the optical approach to sweat monitoring can be very rewarding and solve the main problems of the already implemented colorimetric and electrochemical techniques: expendable compounds and limited monitoring time frames. Furthermore, the wide-spectrum techniques employed in this study actively pinpointed interest spectral regions that can be potentially exploited by other optical sensors. As such, future studies should focus on acquiring and testing optical sensors in the explored IR range as the results from this study show different IR wavelengths of increased importance for some of the most relevant sweat components. Furthermore, it is also crucial to address the NaCl effect in the ATR-FTIR spectroscopy sweat spectrum by creating linear regressions for other sweat biomarkers to further validate the NaCl effect hypothesis.

Regarding the sensors, the most relevant sensors used in this work were the AS7262, the AS7263 and the MAX30101. Future studies should further validate the usability of these sensors by assessing their performance using real human sweat and comparing it to the artificial sweat's performance.

It is also important to note that, despite the almost inexistent absorbance spectrum values produced by the UV-VIS spectrophotometer in the visible light range, all the determined suitable sensors for sweat monitoring (AS7262, AS7263 and MAX30101) operated within the UV-VIS spectral range. This discrepancy within the same spectral range could be attributed to the different operating principles of the explored techniques: absorbance and reflectance. In this sense, future studies should seek a spectral analysis of the artificial sweat or a sweat biomarker solution, in the visible spectrum, using a reflectance spectrophotometry system.

Finally, the optical fiber setup did not possess the needed sensitivity for the artificial sweat measurements. In this light, future work should aim at improving the optic fiber resolution with the aid of, for example, optical fiber microlenses or other equipment that would improve the resolution capacity of the optical fiber.

References

[1] Y. V. Natochin and T. V. Chernigovskaya, “Evolutionary physiology: History, principles,” *Comparative Biochemistry and Physiology - A Physiology*. 1997.

[2] M. J. Patterson, S. D. R. Galloway, and M. A. Nimmo, “Variations in regional sweat composition in normal human males,” *Exp. Physiol.*, 2000.

[3] R. M. Morgan, M. J. Patterson, and M. A. Nimmo, “Acute effects of dehydration on sweat composition in men during prolonged exercise in the heat,” *Acta Physiol. Scand.*, no. 182, pp. 37–43, 2004.

[4] S. Binu, V. P. Mahadevan Pillai, V. Pradeepkumar, B. B. Padhy, C. S. Joseph, and N. Chandrasekaran, “Fibre optic glucose sensor,” *Mater. Sci. Eng. C*, vol. 29, no. 1, pp. 183–186, 2009.

[5] D. Morris, S. Coyle, Y. Wu, K. T. Lau, G. Wallace, and D. Diamond, “Bio-sensing textile based patch with integrated optical detection system for sweat monitoring,” *Sensors Actuators, B Chem.*, vol. 139, no. 1, pp. 231–236, 2009.

[6] S. DeMeulenaere, “Pulse Oximetry: Uses and Limitations,” *J. Nurse Pract.*, 2007.

[7] G. E. Folk and A. Semken, “The evolution of sweat glands,” *Int. J. Biometeorol.*, vol. 35, no. 3, pp. 180–186, 1991.

[8] C. B. Wenger, “Heat of evaporation of sweat: thermodynamic considerations.,” *J. Appl. Physiol.*, vol. 32, no. 4, pp. 456–459, 2017.

[9] M. Shibasaki and C. G. Crandall, “Mechanisms and controllers of eccrine sweating in humans.,” *Front. Biosci. (Schol. Ed).*, 2010.

[10] J. A. Boulant, “Hypothalamic mechanisms in thermoregulation.,” *Fed. Proc.*, 1981.

[11] K. Sato, R. Leidal, and F. Sato, “Morphology and development of an apoeccrine sweat gland in human axillae,” *Am. J. Physiol. Regul. Integr. Comp. Physiol.*, vol. 252, no. 1, pp. R166–R180, 1987.

[12] K. Sato, W. H. Kang, K. Saga, and K. T. Sato, “Biology of sweat glands and their disorders. I. Normal sweat gland function,” *J. Am. Acad. Dermatol.*, vol. 20, no. 4, pp. 537–563, 1989.

[13] P. M. Quinton, “Cystic Fibrosis: Lessons from the Sweat Gland,” *Physiology*, vol. 22, no. 3, pp. 212–225, 2007.

[14] C. Lu and E. Fuchs, “Sweat gland progenitors in development, homeostasis, and wound repair,” *Cold Spring Harb. Perspect. Med.*, vol. 4, no. 2, 2014.

[15] C. Y. Cui and D. Schlessinger, “Eccrine sweat gland development and sweat secretion,” *Exp. Dermatol.*, vol. 24, no. 9, pp. 644–650, 2015.

[16] Z. Sonner *et al.*, “The microfluidics of the eccrine sweat gland, including biomarker partitioning, transport, and biosensing implications,” *Biomicrofluidics*, 2015.

[17] A. B. Stefaniak and C. J. Harvey, “Dissolution of materials in artificial skin surface film liquids,” *Toxicology in Vitro*. 2006.

[18] C. J. Harvey, R. F. Lebouf, and A. B. Stefaniak, “Toxicology in Vitro Formulation and

stability of a novel artificial human sweat under conditions of storage and use," *Toxicol. Vitr.*, vol. 24, no. 6, pp. 1790–1796, 2010.

[19] J. ALONSO Y DE LOS RUYZES DE FONTECA, *Diez Previlegios para Mgeres Prenadas*. Henares, Spain, 1606.

[20] P. M. QUINTON, "Physiological Basis of Cystic Fibrosis: A Historical Perspective," *Physiol. Rev.*, vol. 79, no. 1, pp. S3–S22, 1999.

[21] B. Kerem *et al.*, "Identification of the Cystic Fibrosis Gene: Genetic Analysis," vol. 121, no. August, 1989.

[22] P. M. Farrell *et al.*, "Guidelines for Diagnosis of Cystic Fibrosis in Newborns through Older Adults: Cystic Fibrosis Foundation Consensus Report," *J. Pediatr.*, vol. 153, no. 2, 2008.

[23] C. E. R. Loat and E. C. Rhodes, "Relationship Between the Lactate and Ventilatory Thresholds During Prolonged Exercise," *Sports Medicine: Evaluations of Research in Exercise Science and Sports Medicine*. 1993.

[24] M. L. Goodwin, J. E. Harris, A. Hernández, and L. B. Gladden, "Blood lactate measurements and analysis during exercise: A guide for clinicians," *J. Diabetes Sci. Technol.*, vol. 1, no. 4, pp. 558–569, 2007.

[25] M. M. Cox and D. L. Nelson, "Chapter 14: Glycolysis, Gluconeogenesis, and the Pentose Phosphate Pathway," in *Lehninger Principles of Biochemistry*, W H Freeman & Co, 2008, pp. 527–568.

[26] a Katz and K. Sahlin, "Regulation of lactic acid production during exercise.," *J. Appl. Physiol.*, vol. 65, no. 2, pp. 509–518, 1988.

[27] D. A. Sakharov, M. U. Shkurnikov, M. Y. Vagin, E. I. Yashina, A. A. Karyakin, and A. G. Tonevitsky, "Relationship between lactate concentrations in active muscle sweat and whole blood," *Bull. Exp. Biol. Med.*, vol. 150, no. 7, pp. 94–96, 2010.

[28] T. Ohkuwa, K. Tsukamoto, K. Yamai, H. Itoh, Y. Yamazaki, and T. Tsuda, "The relationship between exercise intensity and lactate concentration on the skin surface," *Int. J. Biomed. Sci.*, vol. 5, no. 1, pp. 23–27, 2009.

[29] M. R. Blanton, J. A. Frieman, and J. Brinkmann, "Sweat Lactic Acid Monitoring System for Assessment of Exercise Intensity," vol. 75, no. 52, pp. 61–66, 2017.

[30] American diabetes association, "Statistics about diabetes," 2015. [Online]. Available: http://www.diabetes.org/diabetes-basics/statistics/. [Accessed: 05-Jan-2019].

[31] J. Moyer, D. Wilson, I. Finkelshtein, B. Wong, and R. Potts, "Correlation Between Sweat Glucose and Blood Glucose in Subjects with Diabetes," *Diabetes Technol. Ther.*, vol. 14, no. 5, pp. 398–402, 2012.

[32] S. K. *et al.*, "Evaluation of a minimally invasive system for measuring glucose area under the curve during oral glucose tolerance tests: Usefulness of sweat monitoring for precise measurement," *J. Diabetes Sci. Technol.*, vol. 7, no. 3, pp. 678–688, 2013.

[33] K. . R. Ashwin, R. K. . Gottlieb, and Q. Ong, "COLOROMETRIC SENSOR FOR THE NON - INVASIVE SCREENING OF GLUCOSE IN SWEAT IN PRE AND TYPE 2 DIABETES," 2018.

[34] H. Lee *et al.*, "Wearable/disposable sweat-based glucose monitoring device with multistage transdermal drug delivery module," *Sci. Adv.*, vol. 3, no. 3, pp. 1–9, 2017.

[35] Y. J. Hong *et al.*, "Multifunctional Wearable System that Integrates Sweat-Based Sensing and Vital-Sign Monitoring to Estimate Pre-/Post-Exercise Glucose Levels," *Adv. Funct. Mater.*, 2018.

[36] Y. Y. Al-Tamer, E. A. Hadi, and I. E. I. Al-Badrani, "Sweat urea, uric acid and creatinine concentrations in uraemic patients," *Urol. Res.*, vol. 25, no. 5, pp. 337–340, 1997.

[37] C. T. Huang, M. L. Chen, L. L. Huang, and I. F. Mao, "Uric acid and urea in human sweat," *Chin. J. Physiol.*, vol. 45, no. 3, pp. 109–115, 2002.

[38] K. B. Pandolf, T. B. Griffin, E. H. Munro, and R. F. Goldman, "Persistence of impaired heat tolerance from artificially induced miliaria rubra," *Am. J. Physiol. Integr. Comp. Physiol.*, 2017.

[39] K. B. Pandolf, T. B. Griffin, E. H. Munro, and R. F. Goldman, "Heat intolerance as a function of percent of body surface involved with miliaria rubra," *Am. J. Physiol. Integr. Comp. Physiol.*, 2017.

[40] F. M. THURMON and B. OTTENSTEIN, "Studies on the chemistry of human perspiration with especial reference to its lactic acid content.," *J. Invest. Dermatol.*, vol. 18, no. 4,

pp. 333–339, 1952.
[41] X. Huang *et al.*, “Stretchable, wireless sensors and functional substrates for epidermal characterization of sweat,” *Small*, vol. 10, no. 15, pp. 3083–3090, 2014.
[42] K. Sakaguchi *et al.*, “A Minimally Invasive System for Glucose Area Under the Curve Measurement Using Interstitial Fluid Extraction Technology: Evaluation of the Accuracy and Usefulness with Oral Glucose Tolerance Tests in Subjects With and Without Diabetes,” *Diabetes Technol. Ther.*, vol. 14, no. 6, pp. 485–491, 2012.
[43] T. Shimomura, T. Sumiya, M. Ono, T. Itoh, and T. Hanaoka, “An Electrochemical Biosensor for the Determination of Lactic Acid in Expiration,” *Procedia Chem.*, vol. 6, pp. 46–51, 2012.
[44] S. S. Kumar, J. Joseph, and K. L. Phani, “Novel method for deposition of gold-prussian blue nanocomposite films induced by electrochemically formed gold nanoparticles: Characterization and application to electrocatalysis,” *Chem. Mater.*, vol. 19, no. 19, pp. 4722–4730, 2007.
[45] A. J. Bandodkar *et al.*, “Epidermal tattoo potentiometric sodium sensors with wireless signal transduction for continuous non-invasive sweat monitoring,” *Biosens. Bioelectron.*, vol. 54, pp. 603–609, 2014.
[46] A. K. Covington, *Ion-Selective Electrode Methodology. Volume I*. CRC Press, 1979.
[47] N. M. S. University, “Ion Selective Electrodes (ISE),” 2006. [Online]. Available: http://web.nmsu.edu/~kburke/Instrumentation/IS_Electrod.html. [Accessed: 18-Jan-2019].
[48] A. Cazalé *et al.*, “Physiological stress monitoring using sodium ion potentiometric microsensors for sweat analysis,” *Sensors Actuators, B Chem.*, vol. 225, pp. 1–9, 2016.
[49] G. Liu, N. Slappey, and S. Snelgrove, “A wearable conductivity sensor for wireless real-time sweat.pdf,” vol. 227, no. B, pp. 35–42, 2016.
[50] S. Haxha and J. Jhoja, “Optical Based Noninvasive Glucose Monitoring Sensor Prototype,” *IEEE Photonics J.*, vol. 8, no. 6, 2016.
[51] T. Takeo and H. Hattori, “Skin hydration state estimation using a fiber-optic refractometer,” *Appl. Opt.*, vol. 33, no. 19, p. 4267, 1994.
[52] J. M. Hollas, *Modern Spectroscopy - Fourth Edition*. 2004.
[53] R. N. Clark, “Reflectance Spectra,” in *AGU Handbook of Physical Constants*, 1995, pp. 178–188.
[54] M. H. Simonian, “Spectrophotometric Determination Of Protein Concentration,” in *Handbook of Food Analytical Chemistry*, 2005.
[55] W.-T. Chu, J. W. Mayer, and M. Nicolet, *BACKSCATTERING SPECTROMETRY*. 1978.
[56] E. Boss and W. S. Pegau, “Relationship of light scattering at an angle in the backward direction to the backscattering coefficient,” *Appl. Opt.*, vol. 40, no. 30, p. 5503, 2001.
[57] R. N. Clark and T. L. Roush, “Reflectance spectroscopy: quantitative analysis techniques for remote sensing applications.,” *J. Geophys. Res.*, vol. 89, no. B7, pp. 6329–6340, 1984.
[58] AMS, “6-Channel Visible Spectral_ID Device with Electronic Shutter and Smart Interface,” *AS7262 Datasheet*, 2017. .
[59] AMS, “6-Channel NIR Spectral_ID Device with Electronic Shutter and Smart Interface,” *AS7263 Datasheet*, 2016. .
[60] Maxim Integrated, “High-Sensitivity Pulse Oximeter and Heart-Rate Sensor for Wearable Health,” *MAX30101 Datasheet*, 2018. .
[61] Maxim Integrated, “MAX30101 Evaluation System,” *MAX30101 evaluation kit Datasheet*, 2016. .
[62] STMicroelectronics, “A new generation, long distance ranging Time-of-Flight sensor based on ST’s FlightSense™ technology,” *VL53L1X Datasheet*, 2018. .
[63] Vishay, “Highbright 0603 ChipLED,” *VLMTG1300 Datasheet*, 2018. .
[64] Vishay, “Dual Color Emitting Diodes, 660 nm and 940 nm,” *VSMD66694 Datasheet*, 2016. .
[65] Vishay, “High Speed Infrared Emitting Diodes, 890 nm, GaAlAs, DH,” *VSMF2890GX01 Datasheet*, 2013. .
[66] Vishay, “Fully Integrated Proximity and Ambient Light Sensor With Infrared Emitter, I2C Interface, and Interrupt Function,” *VCNL4020 Datasheet*, 2018. .
[67] Vishay, “SensorXplorerTM Installation Guide,” *SensorXplorer Datasheet*, 2018. .
[68] D. R. Anderson, L. Johnson, and F. G. Bell, *Troubleshooting Optical Fiber Networks:*

Understanding and Using Your Optical Time-Domain Reflectometer: Second Edition. 2004.
[69] K. Thyagarajan and A. Ghatak, *Fiber Optic Essentials*. 2007.
[70] A. Dutta, "Fourier Transform Infrared Spectroscopy," in *Spectroscopic Methods for Nanomaterials Characterization*, 2017.
[71] J. Grdadolnik, "ATR-FTIR spectroscopy: Its advantages and limitations," *Acta Chim. Slov.*, 2002.
[72] C. K. Jørgensen, *Absorption Spectra and Chemical Bonding in Complexes*. 1962.
[73] A. Toshimitsu, R. Jukka, and P. Kai-Erik, *UV-visible reflection spectroscopy of liquids*, vol. 42, no. 02. 2004.
[74] P. Heinz-Helmut, *UV-VIS Spectroscopy and Its Applications*, vol. 78, no. 11. 1992.
[75] B. W. Chieng, N. A. Ibrahim, W. M. Z. W. Yunus, and M. Z. Hussein, "Poly(lactic acid)/poly(ethylene glycol) polymer nanocomposites: Effects of graphene nanoplatelets," *Polymers (Basel).*, vol. 6, no. 1, pp. 93–104, 2014.
[76] A. Lincoln, S. F.; Richens, D. T. and Sykes, "Metal Aqua Ions," in *Comprehensive Coordination Chemistry II Volume 1*, 2003, pp. 515–555.
[77] M. Schwarzott, D. Baurecht, and U. P. Fringeli, "Solvation effects in aqueous solutions investigated by FTIR-ATR spectroscopy," in *Solutions*, 2001, pp. 4251–4251.
[78] L. Shu, I. J. Obagbemi, V. Jegatheesan, S. Liyanaarachchi, and K. Baskaran, "Effect of multiple cations in the feed solution on the performance of forward osmosis," *Desalin. Water Treat.*, vol. 54, no. 4–5, pp. 845–852, 2015.
[79] W. D. Stein, "Transport and Diffusion across Cell Membranes," *J. Gen. Physiol.*, vol. 71, p. 402, 1978.
[80] A. C. Wilson, G. B. Kitto, and N. O. Kaplan, "Molecular Size of Hagfish Muscle Lactate Dehydrogenase," *Science (80-.).*, vol. 157, no. 3784, pp. 82–83, 1967.
[81] S. J. Perkins, "Protein volumes and hydration effects," *Eur. J. Biochem.*, 1986.